Cellular/Molecular

A Critical Role for Interferon Regulatory Factor 9 in Cerebral Ischemic Stroke

Hou-Zao Chen,[1]* Sen Guo,[2,3]* Zuo-Zhi Li,[1]* Yanyun Lu,[2,3] Ding-Sheng Jiang,[2,3] Ran Zhang,[1] Hao Lei,[4] Lu Gao,[5] Xiaofei Zhang,[6] Yan Zhang,[2,3] Lang Wang,[2,3] Li-Hua Zhu,[2,3] Mei Xiang,[2,3] Yan Zhou,[6] Qi Wan,[7] Hailong Dong,[8] De-Pei Liu,[1] and Hongliang Li[2,3]

[1]State Key Laboratory of Medical Molecular Biology, Department of Biochemistry and Molecular Biology, Institute of Basic Medical Sciences, Chinese Academy of Medical Sciences & Peking Union Medical College, Beijing 100005, China, [2]Department of Cardiology, Renmin Hospital of Wuhan University, Wuhan 430060, China, [3]Cardiovascular Research Institute, Wuhan University, Wuhan 430060, China, [4]Wuhan Center for Magnetic Resonance, State Key Laboratory of Magnetic Resonance and Atomic and Molecular Physics, Wuhan Institute of Physics and Mathematics, Chinese Academy of Sciences, Wuhan 430071, China, [5]Department of Cardiology, Institute of Cardiovascular Disease, Union Hospital, Tongji Medical College, Huazhong University of Science and Technology, Wuhan 430022, China, [6]College of Life Sciences, Wuhan University, Wuhan 430072, China, [7]State Key Laboratory of Virology, Department of Immunology and Hubei Province Key Laboratory of Allergy and Immunology, Wuhan University School of Medicine, Wuhan 430071, China, and [8]Department of Anesthesiology, Xijing Hospital, The Fourth Military Medical University, Xi'an 710032, China

The failure of past efforts to develop effective stroke treatments is at least partially because these treatments often interfered with essential physiological functions, even though they are targeted toward pathophysiological events, such as inflammation, excitotoxicity, and oxidative stress. Thus, the direct targeting of endogenous neuroprotective or destructive elements holds promise as a potential new approach to treating this devastating condition. Interferon regulatory factor 9 (IRF9), a transcription factor that regulates innate immune responses, has been implicated in neurological pathology. Here, we provide new evidence that IRF9 directly mediates neuronal death in male mice. In response to ischemia/reperfusion (I/R), IRF9 accumulated in neurons. IRF9 deficiency markedly mitigated both poststroke neuronal death and neurological deficits, whereas the neuron-specific overexpression of IRF9 sensitized neurons to death. The histone deacetylase Sirt1 was identified as a novel negative transcriptional target of IRF9 both *in vivo* and *in vitro*. IRF9 inhibits Sirt1 deacetylase activity, culminating in the acetylation and activation of p53-mediated cell death signaling. Importantly, both the genetic and pharmacological manipulation of Sirt1 effectively counteracted the pathophysiological effects of IRF9 on stroke outcome. These findings indicate that, rather than activating a delayed innate immune response, IRF9 directly activates neuronal death signaling pathways through the downregulation of Sirt1 deacetylase in response to acute I/R stress.

Key words: **IRF9; stroke; Sirt1; p53; neuroapoptosis**

Introduction

Ischemic stroke is one of the most devastating neurological diseases worldwide and is the leading cause of permanent disability. Currently, there are no effective treatments for ischemic stroke other than tissue plasminogen activator thrombolysis, which is rather limited. The intricate biological pathways that control neuronal death have been extensively investigated in the past two decades (Lo et al., 2003; Lo, 2008; Tymianski, 2011). Various cell death mechanisms, including excitotoxicity, oxidative stress, inflammation, and apoptosis-like cell death, are triggered by cerebral ischemia/reperfusion (I/R) injury, leading to catastrophic histological loss and functional damage (Lo et al., 2003; Moskowitz et al., 2010). Immediately after ischemia, glutamate accumulates at synapses, followed by a dramatically enhanced influx of calcium into neurons and the onset of catabolic processes (Ankarcrona et al., 1995; Lo et al., 2003). The high calcium level in ischemic cells triggers potent oxygen radical production, which directly damages lipids, proteins, nucleic acids, and carbohydrates (Lo et al., 2003). The inflammatory response and apoptosis, which are critical to cell fate in the penumbra, typify the secondary or delayed response to focal ischemia (Broughton et al., 2009; Moskowitz et al., 2010; Chamorro et al., 2012; Lu et al., 2013). Despite tremendous efforts and >1000 clinical trials, the drugs screened based on these approaches have not yielded prac-

Received April 16, 2014; revised July 2, 2014; accepted July 11, 2014.

Author contributions: H. Li and D.-P.L. designed research; H.-Z.C., S.G., Y.L., D.-S.J., Y. Zhang, and M.X. performed research; H. Lei contributed unpublished reagents/analytic tools; L.G., X.Z., L.W., L.-H.Z., Y. Zhou, Q.W., and H.D. analyzed data; Z.-Z.L. and R.Z. wrote the paper.

This work was supported by National Natural Science Foundation of China Grants 81100230, 81070089, 81200071, 81270306, and 81370365, National Science and Technology Support Project 2011BAI15B02, 2012BAI39B05, 2013YQ030923-05, and 2014BAI02B01, the National Basic Research Program of China 2011CB503902, and the Key Project of the National Natural Science Foundation 91339201 and 81330005.

The authors declare no competing financial interests.

*H.-Z.C., S.G., and Z.-Z.L. contributed equally to this work.

Correspondence should be addressed to either of the following: Dr. De-Pei Liu, State Key Laboratory of Medical Molecular Biology, Department of Biochemistry and Molecular Biology, Institute of Basic Medical Sciences, Chinese Academy of Medical Sciences & Peking Union Medical College, No. 5 Dong Dan San Tiao, Beijing 100005, People's Republic of China, E-mail: liudp@pumc.edu.cn; or Dr. Hongliang Li, Department of Cardiology, Renmin Hospital of Wuhan University, Cardiovascular Research Institute, Wuhan University, JieFang Road 238, Wuhan 430060, People's Republic of China, E-mail: lihl@whu.edu.cn.

DOI:10.1523/JNEUROSCI.1545-14.2014

 0270-6474/14/3411897-16$15.00/0

tical results (Labiche and Grotta, 2004; Savitz and Schäbitz, 2008). This failure may be largely due to adverse side effects resulting from their interference with essential physiological events. Thus, to circumvent this roadblock, information on the signaling pathways that are directly involved in neuronal death is urgently needed. Intriguingly, Vaseva et al. (2012) recently reported that the interaction between cyclophilin D and p53 evokes stroke-induced tissue necrosis in the brain. Nevertheless, the need to identify novel determinants of neuronal death remains, and insight into their interplay remains to be explored.

Interferon (IFN) regulatory factors (IRFs) constitute a group of proteins with nine members (IRF1–9) that were first recognized as transcriptional regulators of type I IFNs and IFN-inducible genes (Paun and Pitha, 2007; Tamura et al., 2008; Yanai et al., 2012). IRF9 is constitutively expressed and can be induced by IFN-γ (Ousman et al., 2005; Tamura et al., 2008). In addition, IFN-α/β stimulation may facilitate the formation of IFN-stimulated gene factor 3 (ISGF3), which comprises IRF9 and signal transducer and activator of transcription 1 (STAT1) and 2 (STAT2). ISGF3 binds to the IFN-stimulated response elements (ISREs) of Type I IFN-inducible genes (Darnell et al., 1994; Taniguchi and Takaoka, 2002). In addition to its role in the induction of host defense mechanisms, IRF9 may also link pathological stress with cell fate. For example, *IRF9-RNAi*, but not *Stat1-RNAi*, inhibits IFN-α-induced apoptosis (Tsuno et al., 2009). Furthermore, *p53* transcription cannot be induced by IFN-α/β in the absence of IRF9 (Takaoka et al., 2003). Interestingly, IRF9 may have additional functions beyond IFN signaling. We previously demonstrated that IRF9 may regulate metabolic dysfunction through the coactivation of the peroxisome proliferator-activated receptor α (PPARα) pathway (Wang et al., 2013c) and cardiac hypertrophy (Jiang et al., 2014). More importantly, several recent studies have shown that IRF9 is involved in pathophysiological events in the CNS, such as viral infection and IFN induction (Ousman et al., 2005; Hofer et al., 2010). However, the role of IRF9 in ischemic stroke is presently unknown.

The current study revealed a pathological role for IRF9 in stroke. More importantly, IRF9 was found to be a negative transcriptional regulator of Sirt1, a previously recognized cerebroprotective factor that plays an active role during ischemia. In response to I/R, IRF9 decreased Sirt1 activity and increased the acetylation of p53, resulting in increased ischemic damage. Correspondingly, both the genetic and pharmacological manipulation of Sirt1 effectively ameliorated the pathophysiological effects of IRF9 on stroke outcome. Thus, the IRF9/Sirt1 pathway is implicated in I/R injury.

Materials and Methods

Animals. All experiments with mice were performed in accordance with protocols approved by the Animal Care and Use Committee of Renmin Hospital of Wuhan University. Global *IRF9* knock-out mice (*IRF9*$^{-/-}$, C57BL/6J background) were kindly provided by Dr. Tadatsugu Taniguchi (Department of Immunology, Graduate School of Medicine and Faculty of Medicine, University of Tokyo) (Wang et al., 2013c). Neuron-specific *Cre* transgenic mice (*CaMKII*α*-Cre*; stock #005359) were purchased from The Jackson Laboratory. Genotyping of mouse strains was performed using the following primers: *CaMKII*α*-Cre* forward: 3′-GCGGTCTGGCAGTAAAAACTATC-5′; *CaMKII*α*-Cre* reverse: 3′-GTGAAACAGCATTGCTGTCACTT-5′. *Sirt1*$^{flox/flox}$ homozygous mice were generated by inserting a *loxP*-flanked neomycin cassette upstream of exon 4 of the targeted gene and a third *loxP* site downstream of exon 4, as previously described (Chen et al., 2008). The addition of the *loxP* sites does not affect Sirt1 expression in homozygous mice. When these mice are crossed with *CaMKII*α*-Cre* mice that express neuron-specific *Cre* recombinase, exon 4 is deleted in the neurons of the resulting offspring (*Sirt1*-KO). The following primers were used for the PCR genotyping of *Sirt1*$^{flox/flox}$ and *Sirt1*-KO mice: primer 1, 5′-GGTTGACTTAGGTCTTGTCTG-3′; primer 2, 5′-CGTCCCTTGTAATGTTTCCC-3′; and primer 3, 5′-AGGCGGATTTCTGAGTTCGA-3′. Primer 1 and primer 2 were used to genotype the *Sirt1*$^{flox/flox}$ mice, and primer 2 and primer 3 were used to genotype the *Sirt1*-KO mice. Full-length mouse *IRF9* cDNA was inserted into the *CAG-CAT-LacZ* construct, which contains a *CMV* enhancer and a chicken β-actin gene (*CAG*) promoter, and then linked to the chloramphenicol acetyltransferase (*CAT*) gene flanked by *loxP* sites. *IRF9-floxed* mice were produced by microinjecting the construct into fertilized embryos (C57BL/6J background). Neuron-specific *IRF9* transgenic mice (*IRF9*-TG) were produced by crossing *IRF9-floxed* mice with *CaMKII*α*-Cre* mice. *GFAP-cre* (stock #012887) and *Lyz-Cre* (stock #004781) mice were both purchased from The Jackson Laboratory. These two mouse lines were crossed with *IRF9-floxed* mice to generate microglia- and astrocyte-specific *IRF9* transgenic mice, respectively. Similar procedures were used to obtain neuron-specific *Sirt1* transgenic mice (*Sirt1*-TG, C57BL/6J background). *IRF9*$^{-/-}$ mice were crossed with *Sirt1*-KO mice to produce *IRF9*$^{-/-}$/*Sirt1*-KO double-knock-out mice (DKO, C57BL/6J background), and *Sirt1*-TG and *IRF9*-TG mice were crossed to generate *IRF9/Sirt1* double-transgenic mice (DTG, C57BL/6J background). All of the mice were housed in an environment with controlled light (12 h light/12 h dark), temperature and humidity, with food and water available *ad libitum*. All the mice used in this study were male and aged from 11 to 12 weeks (25–30 g), and all of the animal experiments were performed by an experimenter who was blinded to the genotypes.

Administration of the Sirt1 inhibitor or activator in vivo. The Sirt1 inhibitor EX527 (2780, Tocris Bioscience) was dissolved in DMSO and diluted to the final concentration with normal saline (15 μl; the final DMSO concentration was $<$2%). We intracranially injected EX527 into wild-type (WT) and *IRF9* knock-out (*IRF9*-KO) mice 30 min before the onset of middle cerebral arterial occlusion (MCAO) at a dose of 30 μg. Antithetically, the nontransgenic (NTG) and neuron-*IRF9*-TG mice were intracranially injected with the Sirt1 agonist SRT1720 (S1129, Selleck), which was prepared in parallel with EX527 30 min before the onset of MCAO at a dose of 30 μg. An identical volume of DMSO was injected intracranially as a control.

Brain ischemia/reperfusion induced by surgical MCAO. Cerebral ischemia was induced by transient 45-min left-middle MCAO in mice under isoflurane anesthesia as previously described (Wang et al., 2012a, b, 2013a, b). In brief, the mice were maintained at a rectal temperature of 37 $\pm$ 0.5°C using a heating plate. The left common carotid artery was exposed, and a 6-0 silicon-coated monofilament (Doccol) was inserted into the internal carotid artery via the external carotid artery. After advancement into the cerebral arterial circle, the filament obstructed the origin of the middle cerebral artery. Doppler analysis (Periflux System 5010; Perimed) was used to monitor the reduction and restoration of regional cerebral blood flow (CBF). After the withdrawal of the filament, CBF was restored for the time periods indicated in the text. The mice were returned to a heated cage for 2 h to recover, with free access to food and water. For the sham-operated controls, the filament was withdrawn immediately after the CBF diminished. We recorded the heart rate, blood gases, systolic blood pressure (SBP), and diastolic blood pressure (DBP) in randomly selected conscious mice. To verify the integrity of the cerebral vasculature, India ink staining was performed, as previously described (Wang et al., 2012b), and the circle of Willis was imaged using a Nikon D700 digital camera. At 24 and 72 h after the induction of MCAO, neurological deficits were tested using the following 9 point scale: (1) absence of neurological deficits (0 points); (2) left forelimb flexion upon suspension by the tail or failure to fully extend the right forepaw (1 point); (3) left shoulder adduction upon suspension by the tail (2 points); (4) reduced resistance to a lateral push toward the left (3 points); (5) spontaneous movement in all directions, with circling to the left only if pulled by the tail (4 points); (6) circling or walking spontaneously only to the left (5 points); (7) walking only when stimulated (6 points); (8) no response to stimulation (7 points); and (9) stroke-related death (8 points) (Xia et al., 2006; Wang et al., 2013b).

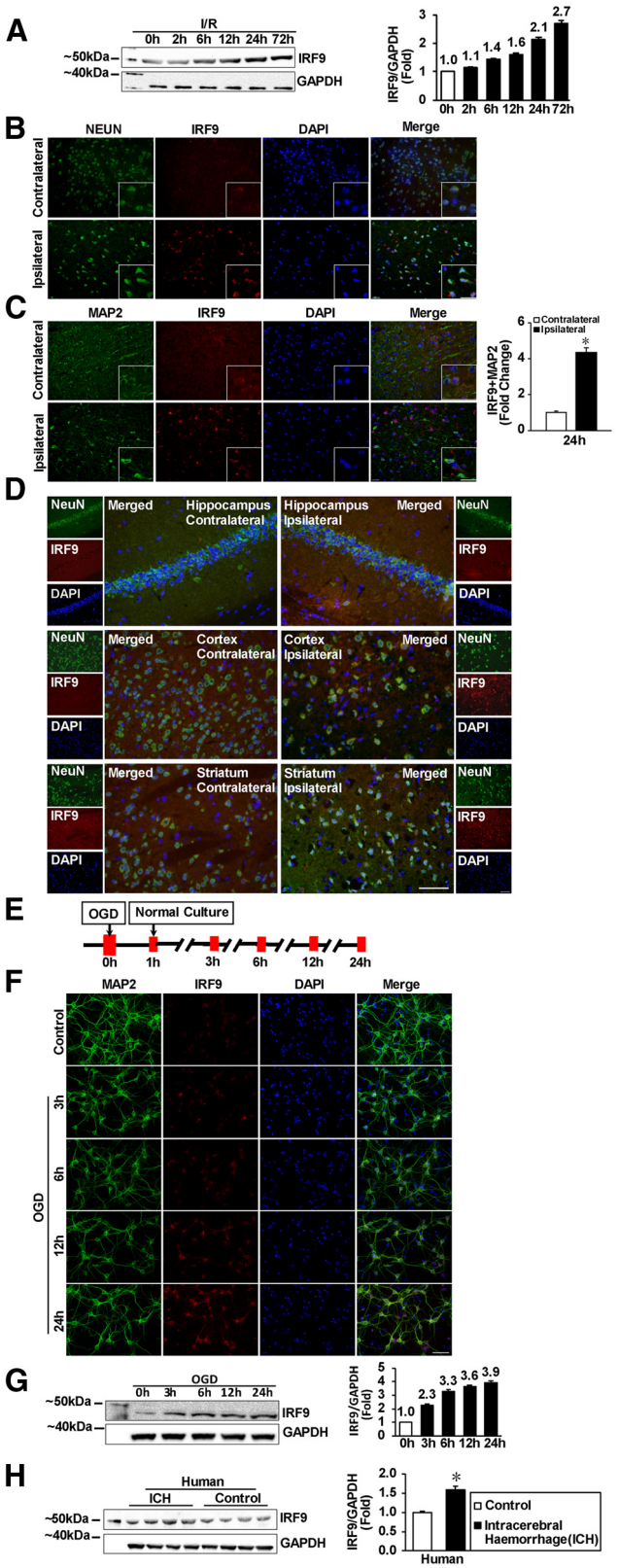

Figure 1. Expression of IRF9 in neurons is elevated in ischemic stroke. ***A***, Immunoblotting of IRF9 in mouse brains before and after I/R for the indicated time points. GAPDH served as a loading control. $n = 3$ per time point. ***B***, ***C***, IRF9 is induced in neurons during stroke. Mouse brains were costained with IRF9 (red) and either (***B***) NEUN (green) or (***C***) MAP2 (green) in both ipsilateral (24 h I/R) and contralateral hemispheres. The nuclei were stained using DAPI. Insets, Images at higher magnification. ***D***, IRF9 (red) and NEUN (green) coimmunohistochemistry of regions of the hippocampus, cortex, and striatum from the ipsilateral (24 h I/R) and contralateral sides (as labeled). Merged images are shown. ***E***, The primary cortical neurons were subjected to OGD/reperfusion for the indicated time points. ***F***, The cells were immunostained for IRF9 (red), MAP2 (green), and DAPI (blue). Scale bar, 50 μm. ***G***, Immunoblotting of IRF9 in cultured primary neurons after OGD/reperfusion for the indicated time points. $n = 4$ per time point. ***H***, Immunoblotting of IRF9 in normal (control) or ICH human brain samples. $n = 4$. *$p <$ 0.05 versus control. Error bars indicate mean ± SE. Scale bars: ***B–D***, ***F***, 20 μm.

Infarct volume quantification. All infarct quantification was performed by a second examiner who was blinded to the genotypes and/or operation. We harvested the brains at 24 h, 72 h, or 7 d after MCAO, and 2% 2,3,5-triphenyl-2H-tetrazolium chloride (TTC) staining was performed as previously described (Wang et al., 2013a, b). Briefly, after being sectioned at 1 mm, a total of seven brain sections were incubated with TTC solution for 15 min at 37°C and then fixed in 10% formalin solution for 8 h. Viable brain tissue was stained red, whereas a pale gray color indicated infarcted tissue. The images were captured and analyzed using Image-Pro Plus (version 6.0). The infarct volume (%) of the seven slices was calculated after correcting for edema, as previously described (Wang et al., 2012a, 2013a, b).

MRI. After anesthetization with chloral hydrate (15307-500G-R, Sigma), the mice were subjected to MRI scanning using a 7.0-T magnetic resonance scanner (BioSpec 70/20USR, Bruker BioSpin). We maintained the temperature using a built-in heating block, and the respiration of the animal was monitored throughout the procedure. The parameters used for imaging were as follows: slice thickness = 0.50 mm, field of view (FOV) = 2 cm, echo time (TE)/repetition time (TR) = 26.7/2000 ms, resolution = 0.078 mm × 0.078 mm, echo train length = 4, number of averages = 4, matrix size = 256 × 256. The percentage of infarct volume was summed (a total of five slices), multiplied by the slice thickness and corrected for edema.

Immunohistology. The following primary antibodies were used for immunohistology: mouse anti-NeuN (MAB377; 1:200; Millipore), chicken anti-MAP2 (Ab5392; 1:100; Abcam), rabbit anti-cleaved caspase-3 (#9661; 1:100; Cell Signaling Technology), anti-IRF9 (sc10793; 1:50; Santa Cruz Biotechnology), and anti-Sirt1 (sc15404; 1:50; Santa Cruz Biotechnology). The following secondary antibodies were used for immunohistology: goat anti-chicken IgY (H&L, DyLight 488, ab96947; Abcam), goat anti-mouse IgG-AlexaFluor-488 conjugate (A11001; Invitrogen), and anti-rabbit IgG-AlexaFluor-568 conjugate (A11011; Invitrogen). All specimens were fixed in 4% PFA in phosphate buffer for 6–8 h at room temperature and incubated overnight at 4°C in phosphate buffer containing 30% sucrose, as previously described (Wang et al., 2012b, 2013a, b). The brains were frozen in optimum cutting temperature compound and sectioned at 5 μm. Neuronal cells were cultured on coverslips and fixed with ice-cold acetone. The cryosections or coverslips were blocked in PBS containing 10% goat serum and incubated overnight with the primary antibody at 4°C. After several PBS rinses, the indicated secondary antibodies were applied for 1 h. The nuclei were stained with DAPI (S36939, Invitrogen). A TUNEL assay was performed using an ApopTag Plus In Situ Apoptosis Fluorescein Detection Kit (S7111; Millipore) according to the manufacturer's protocol. The TUNEL-positive cells were evaluated under microscopy and quantified under high-power magnification (200×). To detect I/R-induced neuronal degeneration, the brain sections were stained with Fluoro-Jade B (AG310, Millipore) according to the manufacturer's instructions. The images were acquired with a fluorescence microscope (OLYMPUS DX51) and DP2-BSW software (version 2.2) and analyzed using Image Pro Plus (version 6.0).

Tissue preparation. The mice were transcardially perfused, and the brains were immediately removed. An experimenter, blinded to the genotype, then excised the olfactory bulbs and 1 mm sections of the anterior and posterior brain tissue. The remaining tissues of the ipsilateral (including the infarct and peri-infarct areas) and contralateral (normal) hemispheres were harvested and immediately frozen in liquid nitrogen and stored at −80°C.

Quantitative real-time PCR. RNA was extracted using TRIzol reagent (11667165001, Roche) following the manufacturer's instructions. cDNA

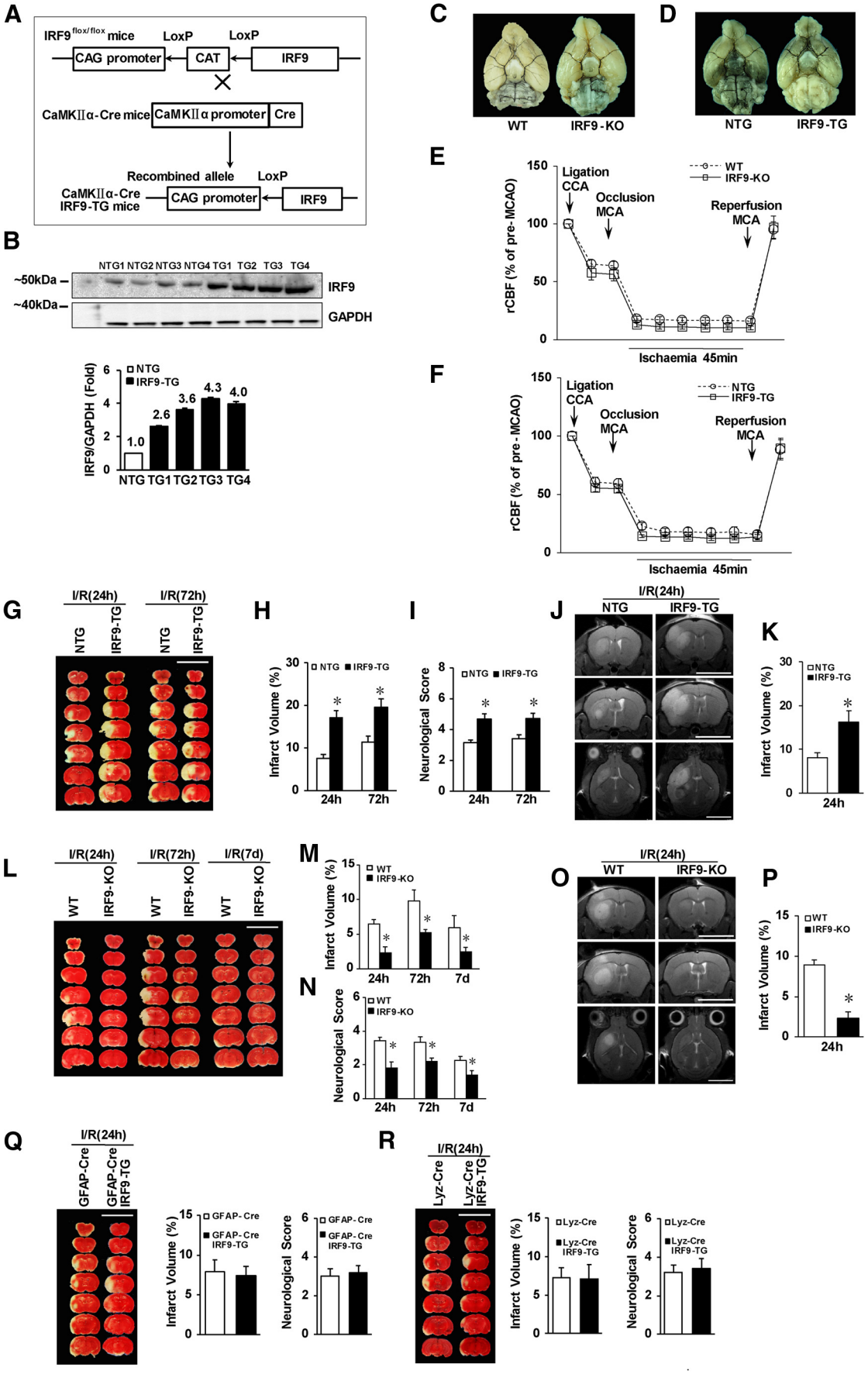
A
IRF9flox/flox mice
LoxP
LoxP
CAG promoter
CAT
IRF9
CaMKIIα-Cre mice
CaMKIIα promoter
Cre
Recombined allele
LoxP
CaMKIIα-Cre IRF9-TG mice
CAG promoter
IRF9
B
NTG1 NTG2 NTG3 NTG4 TG1 TG2 TG3 TG4
~50kDa
~40kDa
IRF9
GAPDH
IRF9/GAPDH (Fold)
NTG
IRF9-TG
1.0
2.6
3.6
4.3
4.0
NTG TG1 TG2 TG3 TG4
C
WT
IRF9-KO
D
NTG
IRF9-TG
E
Ligation CCA
Occlusion MCA
Reperfusion MCA
WT
IRF9-KO
rCBF (% of pre-MCAO)
Ischaemia 45min
F
Ligation CCA
Occlusion MCA
Reperfusion MCA
NTG
IRF9-TG
rCBF (% of pre-MCAO)
Ischaemia 45min
G
I/R(24h)
I/R(72h)
NTG
IRF9-TG
H
Infarct Volume (%)
NTG
IRF9-TG
24h
72h
I
Neurological Score
NTG
IRF9-TG
24h
72h
J
I/R(24h)
NTG
IRF9-TG
K
Infarct Volume (%)
NTG
IRF9-TG
24h
L
I/R(24h)
I/R(72h)
I/R(7d)
WT
IRF9-KO
M
Infarct Volume (%)
WT
IRF9-KO
24h
72h
7d
N
Neurological Score
WT
IRF9-KO
24h
72h
7d
O
I/R(24h)
WT
IRF9-KO
P
Infarct Volume (%)
WT
IRF9-KO
24h
Q
I/R(24h)
GFAP-Cre
GFAP-Cre IRF9-TG
Infarct Volume (%)
GFAP-Cre
GFAP-Cre IRF9-TG
Neurological Score
GFAP-Cre
GFAP-Cre IRF9-TG
R
I/R(24h)
Lyz-Cre
Lyz-Cre IRF9-TG
Infarct Volume (%)
Lyz-Cre
Lyz-Cre IRF9-TG
Neurological Score
Lyz-Cre
Lyz-Cre IRF9-TG

Table 1. Physiological variables of WT, IRF9-KO, NTG, and IRF9-TG mice before MCAO[a]

	WT	IRF9-KO	NTG	IRF9-TG
pH	7.298 ± 0.027	7.330 ± 0.032	7.343 ± 0.018	7.293 ± 0.058
pO_2 (mmHg)	109.40 ± 3.64	118.75 ± 3.17	115.25 ± 1.38	116.25 ± 4.80
pCO_2 (mmHg)	38.40 ± 2.23	34.25 ± 3.25	38.50 ± 3.43	38.00 ± 5.12
DBP (mmHg)	109.12 ± 2.68	107.73 ± 3.19	104.37 ± 2.14	103.18 ± 0.81
SBP (mmHg)	133.88 ± 4.82	133.97 ± 4.81	134.76 ± 1.59	130.57 ± 1.88
Heart rate (b.p.m.)	612.93 ± 25.66	629.40 ± 7.31	635.36 ± 11.50	621.53 ± 17.80

[a]The pH, pO_2, pCO_2, blood pressure, and heart rate were detected before MCAO. No significant differences were observed between groups. $n = 4$ or 5.

synthesis was conducted using a Transcriptor First Strand cDNA Synthesis Kit (04897030001, Roche). Quantitative RT-PCR analysis was performed using the LightCycler 480 SYBR Green I Master Mix (04887352001, Roche) and the LightCycler 480 QPCR System (Roche). The relative quantity of the mRNAs was calculated after being normalized to GAPDH. The following primer pairs were used: *Sirt1* forward, 5′-TGGAGCAGGTTGCAGGAATCCA-3′; *Sirt1* reverse, 5′-TGGCTTCATGATGGCAAGTGGC-3′; *Bax* forward, 5′-TGAGCGAGTGTCTCCGGCGAAT-3′; *Bax* reverse, 5′-GCACTTTAGTGCACAGGGCCTTG-3′; *Noxa* forward, 5′-ATAACTGTGGTTCTGGCGCA-3′; *Noxa* reverse, 5′-CAATCCTCCGGAGTTGAGCA-3′; *Puma* forward, 5′-ACGACCTCAACGCGCAGTA-3′; *Puma* reverse, 5′-TAGTTGGGCTCCATTTCTGG-3′; *Irf9* forward, 5′-ACAACTGAGGCCACCATTAGAGA-3′; and *Irf9* reverse, 5′-CACCACTCGGCCACCATAG-3′.

RNA sequencing. Total RNA was extracted from brain tissues in WT and *IRF9*-KO mice as described above. RNAs were sequenced using an Illumina HiSeq 2000 instrument at Beijing Genomics Institute (BGI).

Immunoblotting. The following antibodies were used for immunoblotting: rabbit anti-cleaved caspase-3 (Asp 175; #9661), anti-caspase-3 (#9662), anti-Bax (#2772), anti-GAPDH (2118), anti-Bcl2 (2870), and anti-Cyto.c (4280) (all from Cell Signaling Technology; 1:1000); anti-IRF9 (sc10793), anti-Sirt1 (sc15404), anti-Noxa (sc30209), and anti-COX2 (sc23983) (all from Santa Cruz Biotechnology); anti-acetyl-p53 (ab52172), anti-Puma (ab54288), and anti-LDH (ab53010) (all from Abcam); anti-p53 (BS1565, Bioworld); peroxidase-AffiniPure goat anti-mouse IgG (H+L) (115-035-003) and peroxidase-AffiniPure goat anti-rabbit IgG (H+L) (111-035-003) (both from Jackson ImmunoResearch Laboratories). Finally, Western blotting was performed as previously described, and proteins were visualized using a FluorChem E (Cell Biosciences) imaging system (Wang et al., 2013a, b). Briefly, we extracted the peri-infarct cortex, defined as the cortical area within a 2.5 mm radius from the stroke core. The brain extract or cultured cells were lysed using lysis buffer. A total of 20 μg of protein was loaded into each lane, separated on a 10% SDS-PAGE gel (NP0301BOX, Invitrogen), and transferred onto a PVDF membrane (IPVH00010, Millipore). The membranes were incubated in blocking buffer (TBS containing 5% skim milk powder) for 90 min at room temperature and incubated overnight at 4°C with the primary antibodies. The membranes were then washed and incubated with the secondary antibodies before signal detection. Mouse anti-GAPDH served as the internal control.

Primary cell culture and in vitro *studies.* The brains of Sprague Dawley rats were removed within 1–2 d of birth to obtain primary cortical neurons, as described previously (Wang et al., 2013a, b). Briefly, rat cortices were incubated with 2 ml of 0.125% trypsin (Invitrogen) for 20 min at 37°C and neutralized in 4 ml of DMEM/F-12 (Invitrogen) containing 20% FBS (Invitrogen). After centrifuging for 5 min at 1000 rpm, the pellet was resuspended in the same DMEM/FBS solution. The neurons were filtered and seeded on plates coated with poly-L-lysine (10 mg/ml, Sigma) before being cultured in neurobasal medium (Invitrogen) supplemented with B27 (Invitrogen) and AraC (5 μM, Sigma). After 5 d in culture, the neurons were subjected to oxygen-glucose deprivation (OGD) (serum-free, glucose-free Locke's buffer; 95% N_2 and 5% CO_2, pH 7.2) for 60 min in an experimental hypoxia chamber and returned to normal culture conditions for the indicated periods. Neurons cultured in neurobasal medium in a normal oxygen-conditioned incubator (95% air, 5% CO_2) for the same periods as the experimental cells served as controls. In some experiments, we preincubated the cells with the Sirt1 inhibitors nicotinamide (V900517-250G, Sigma) and EX527 (2780, Tocris Bioscience) together with the Sirt1 activators resveratrol (1418, Tocris Bioscience) and SRT1720 (S1129, Selleck) for 30 min before the neuronal cultures were subjected to OGD/reperfusion. Nicotinamide, EX527, resveratrol, and SRT1720 were used at a concentration of 5 μM in the *in vitro* experiments. An identical volume of DMSO was used as the control.

Sirt1 deacetylase activity assays. Sirt1 deacetylase activity was determined with a SIRT1 Fluorometric Drug Discovery Kit (BIOMOL International) following the manufacturer's protocol. Brain and cell extracts were incubated for 80 min at 37°C with Sirt1 substrate reagent and nicotinamide adenine dinucleotide $^+$. The deacetylase activity was detected as a fluorescent signal at 460 nm with an excitation wavelength at 405 nm using a spectrophotometer.

Plasmid constructs and transfection. To generate *Myc*-tagged *IRF9*, we first amplified the murine *IRF9* gene-encoding region with primers 5′-CCGGAATTCATGGCATCAGGCAGGGCACG-3′ and 5′-CCGCTCGAGCTACACCAGGGACAGAATGGCTG-3′ using HA-*IRF9* vector as a template. The murine *IRF9* protein-coding sequence was then inserted into the Myc-C1 vector to obtain *Myc-IRF9*. Transient transfection was conducted using a FuGENE transfection reagent (E2312; Promega) according to the manufacturer's instructions.

Recombinant adenoviral vectors. We constructed adenoviruses carrying sequences encoding rat *IRF9* (*AdIRF9*) and *Sirt1* (*AdSirt1*) as well as short hairpin RNAs targeting *IRF9* (*shIRF9*) or *Sirt1* (*AdshSirt1*) for the *in vitro* studies. *AdIRF9* and *AdshIRF9* were generated as described previously (Wang et al., 2013c). Replication-defective adenoviral vectors were used to overexpress rat *Sirt1* (*AdSirt1*) under the control of the *CMV* promoter, and a similar adenoviral vector expressing GFP was used as a control. To knock down Sirt1 expression, three SureSilencing mouse *shSirt1* constructs were obtained from SABiosciences (KM05054G), and the construct that produced the most significant reduction in Sirt1 levels was selected for further experiments (designated as AdshSirt1). The cultured cortical neurons were transfected with adenovirus at an MOI of 100 for 24 h.

Cell viability. To examine cell viability, a nonradioactive cell counting kit-8 (CCK-8) assay (CK04, Dojindo) and a colorimetric LDH cytotoxicity assay (G1780, Promega) were used according to the manufacturer's protocols. At least three independent experiments were performed by a second examiner who was blinded to the treatments.

Dual luciferase-reporter assay. Adenovirus encoding *Sirt1*-luc was generated by inserting the 1470 bp *Sirt1* promoter region into the *pGL3*-basic vector (Promega) using the primers 5′-CCGCTCGAGCCCTCCTCCCTCGCCTCCT-3′ (forward) and 5′-CCGACGCGTCCTAATGCTCTCCCTCCCCT-3′ (reverse). This vector was then recombined with the *pAdEasy* backbone vector as described above. The primary cortical neurons were cultured in 24-well plates, and cells at 50%–80% confluence were infected with the indicated recombinant adenoviruses. A re-

←

Figure 2. Characteristics of IRF9-KO and IRF9-TG mice; neuronal IRF9 exacerbates poststroke cerebral injury. ***A***, The generation of IRF9-TG mice. ***B***, A representative Western blot of IRF9 in IRF9-TG mice. GAPDH served as the loading control. ***C***, ***D***, Representative images showing the integrity of the cerebral vasculature stained with India ink in IRF9-KO (***C***) and IRF9-TG mice (***D***). $n = 3$–5. ***E***, ***F***, rCBF in WT and IRF9-KO (***E***) and NTG and IRF9-TG mice (***F***) was detected by Doppler before and after I/R, respectively ($n = 6$ or 7, $p > 0.05$ between strains). ***G***, TTC-stained sections from NTG and IRF9-TG mice at 24 and 72 h after I/R. ***H***, ***I***, Quantification of infarct volumes (***H***) and neurological deficit scores (***I***) 24 and 72 h after I/R. $n = 5$–7 per time point. $^*p < 0.05$ versus NTG mice. ***J***, A representative MRI image of mouse brains 24 h after I/R. ***K***, Quantification of infarct volumes in ***J***. $n = 4$ or 5. $^*p < 0.05$ versus NTG. ***L***, TTC-stained sections from WT and IRF9-KO mice at the indicated times after I/R. ***M***, ***N***, Quantification of the infarct volumes (***M***) and neurological deficit scores (***N***) 24 h, 72 h, or 7 d after I/R. $n = 4$–7 per time point. $^*p < 0.05$ versus WT mice. ***O***, MRI images of mouse brains 24 h after I/R. ***P***, Quantification of the infarct volumes. $n = 3$. $^*p < 0.05$ versus WT. Error bars indicate mean ± SE. Scale bars: ***G***, ***L***, 10 mm; ***J***, ***O***, 5 mm. ***Q***, ***R***, TTC-stained sections and quantification of infarct volumes and neurological deficit scores from GFAP-Cre and astrocyte-specific IRF9-transgenic (GFAP-Cre/IRF9-TG) mice (***Q***) and Lyz-Cre and microglia-specific IRF9-transgenic (Lyz-Cre/IRF9-TG) mice (***R***) at 24 h after I/R. $n = 5$–7.

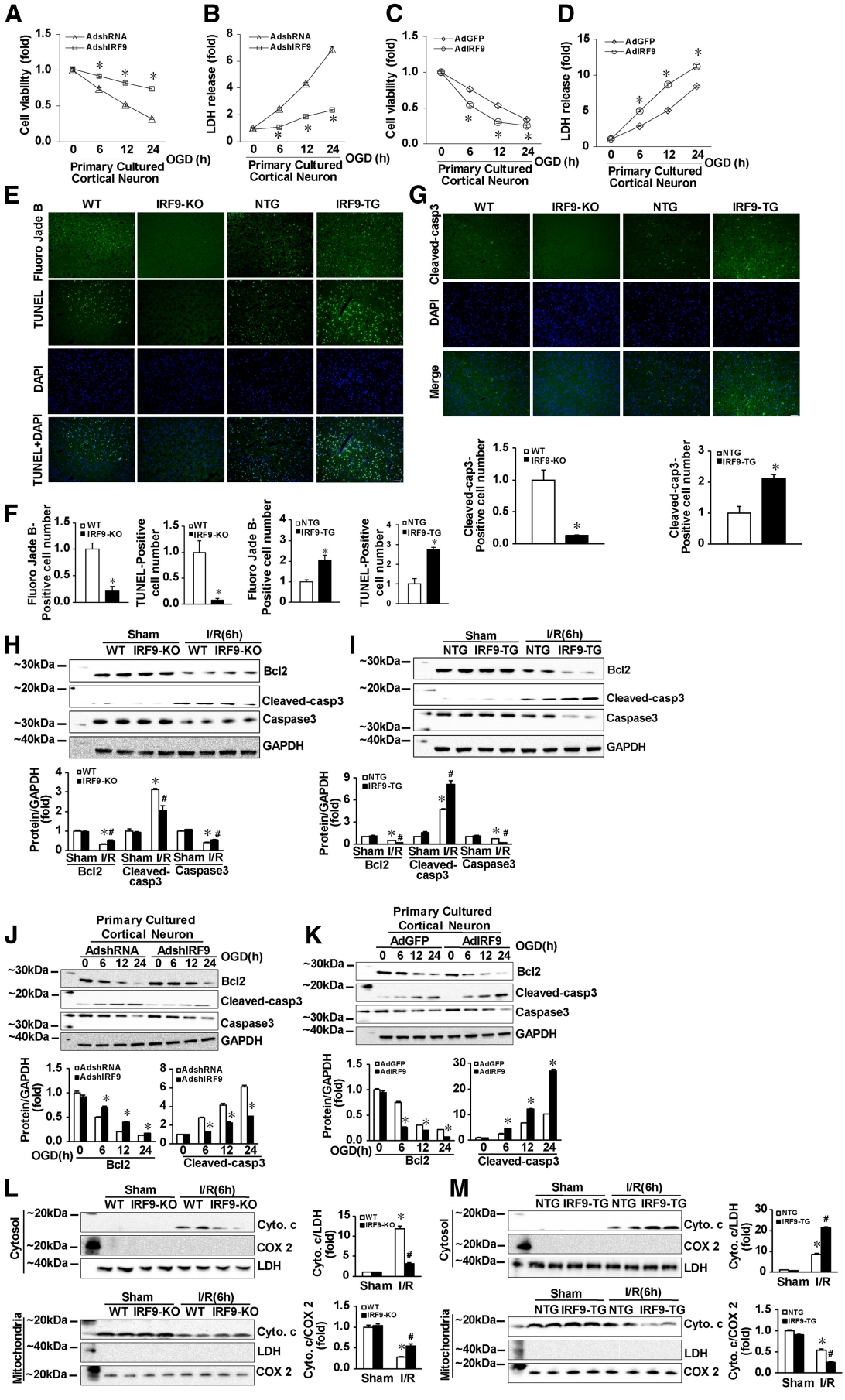
A
Cell viability (fold)
AdshRNA
AdshIRF9
Primary Cultured Cortical Neuron
OGD (h)
B
LDH release (fold)
C
Cell viability (fold)
AdGFP
AdIRF9
D
LDH release (fold)
E
WT
IRF9-KO
NTG
IRF9-TG
Fluoro Jade B
TUNEL
DAPI
TUNEL+DAPI
G
Cleaved-casp3
Merge
Cleaved-cap3-Positive cell number
F
Fluoro Jade B-Positive cell number
TUNEL-Positive cell number
H
Sham
I/R(6h)
~30kDa
~20kDa
~40kDa
Bcl2
Cleaved-casp3
Caspase3
GAPDH
Protein/GAPDH (fold)
Sham I/R
Bcl2
Cleaved-casp3
Caspase3
I
J
Primary Cultured Cortical Neuron
AdshRNA
AdshIRF9
OGD(h)
K
AdGFP
AdIRF9
L
Cytosol
Mitochondria
Cyto. c
COX 2
LDH
Cyto. c/LDH (fold)
Cyto. c/COX 2 (fold)
M

Table 2. Sirt1 and indicated Sirt1-targeted genes in brains of IRF9-KO mice compared with WT control[a]

Sirt1 targets	Transcript ID	Symbol	Log2 ratio (case/control)
Sirt1	NM_019812	Sirt1	2.135
	NM_008117	Gh	2.574
	NM_008709	MYCN	1.558
Proliferation and growth	NM_007415	PARP1	2.976
	NM_007527	BAX	−1.69
	NM_007609	CASP4	−1.834
	NM_007656	CD82	−1.741
	NM_007833	DCN	−1.465
	NM_010107	EFNA1	−1.494
	NM_019740	FOXO3	−1.552
	NM_008655	GADD45B	−1.697
Cell-cycle arrest and apoptosis	NM_001037713	XAF1	−3.031
	NM_007913	EGR1	1.508
	NM_008882	PLXNA2	1.811
Neuronal formation and function	NM_001111015	SYN2	1.401
	NM_011888	CCL19	−1.769
	NM_011611	CD40	−1.423
	NM_021274	CXCL10	−5.304
	NM_011163	EIF2AK2	−2.062
	NM_010260	Gbp2	−3.44
	NM_001111282	HMGB1	−1.564
	NM_001033450	Ifi204	−5.145
	NM_027835	IFIH1	−1.674
	NM_008361	IL1B	−3.019
	NM_031168	IL6	−2.724
	NM_016850	IRF7	−2.006
	NM_001113527	ISG20	−1.553
	NM_008605	MMP12	−1.99
	NM_019401	NMI	−1.508
	NM_016764	PRDX4	−1.59
Immune response and inflammation	NM_009283	STAT1	−1.595
	NM_010856	Myh6	5.259
	NM_001111279	Wdfy1	4.47
	NM_053200	Ces3	−3.621
Other	NM_019697	Kcnd2	−1.99

[a]IRF9 ablation alters the expressions of Sirt1-targeted genes. Log2 ratio of mRNA levels of Sirt1 and indicated Sirt1-targeted genes in brains of IRF9-KO mice compared with WT control, as determined by three independent mRNA microarray experiments.

combinant adenovirus of *pRL-TK* was coinfected as an infection efficiency control, and the luciferase activities were normalized based on the TK activities. After 24 h, the neuronal cultures were subjected to OGD for the indicated times before harvesting. The cells were lysed with 100 μl of passive lysis buffer (Promega) at room temperature. After centrifuging, the supernatant was collected and assessed for luciferase activity using a Single-Mode SpectraMax Microplate Reader, as described previously. The values were normalized to the activity from the cotransfected *Renilla* luciferase expression vector.

Chromatin immunoprecipitation (ChIP) protocol. In brief, after they were transfected with *Myc*-tagged *IRF9* or *pc.DNA3.1* control for 48 h, the cultured N2A cells were fixed with 1% formaldehyde for 10 min. Cross-linking was stopped by adding 1 ml ice-cold glycine at room temperature, and the cells were washed, harvested, and sonicated on ice. After the lysate was precleared with protein G/A beads, the soluble chromatin was immunoprecipitated using anti-Myc antibody (11814150001, Roche) or rabbit IgG (2729S, Cell Signaling Technology) as a control at 4°C overnight with rotation. The chromatin was then eluted from the beads and reverse cross-linked overnight, and then the precipitated DNAs were purified using phenol/chloroform extraction. Real-time quantitative PCR was performed for 40 cycles to detect putative IRF9 binding regions (see Fig. 4*J*, P1-P5). The following primer pairs were used for ChIP assays: P1 forward, 5′-CATTCTGCCTCCTGAGTGCTAA3′; P1 reverse, 5′-GTGGCTCACAACCACCTGTAAC-3′; P2 forward, 5′-GGCTTGCTGGTGTACATCTT-3′; P2 reverse, 5′-TGGTAAACACAGACATGTATGG-3′; P3 forward, 5′-AAACCTGACTAGCTGATTTCTC-3′; P3 reverse, 5′-GTAAGTTGAAGGTAATCTCCAA-3′; P4 forward, 5′-TCCTCAATCGCCAGATCTTTC-3′; P4 reverse, 5′-TTCCTGAGGAGAACTCCTCCA-3′; P5 forward, 5′-AGGTGGCGCTCGCCCTTCA-3′; and P5 reverse, 5′-CCACTGCTGCGCTCGGCTC-3′.

Human brain tissue samples. Research with human brain tissues was approved by the ethics committee of the Xijing Hospital of Fourth Military Medical University. Human samples were derived from a total of 4 male patients with fatal intracerebral hemorrhage (ICH); the contralateral hemisphere, where hemorrhagic lesions were absent, served as controls. Briefly, on biopsy, the hemorrhagic area was removed and 1 cm^3 of adjacent perihematomal brain tissue was obtained by an experienced neuropathologist. All of the samples were acquired, frozen in liquid nitrogen, and stored at −80°C within the first 6 h after death to avoid tissue degradation.

Statistical analyses. The data are presented as mean ± SE. Differences between the groups were determined using ANOVA followed by a *post hoc* Tukey's test. Comparisons between two groups were performed using an unpaired Student's *t* test with the significance set at $p < 0.05$. All *in vivo* and imaging studies were performed in a blinded manner.

Results

IRF9 accumulates in ischemic cerebral tissue

IRF9 expression can be induced in the CNS by several forms of stress, including viral infection and axonal transection (Ousman et al., 2005; Khorooshi and Owens, 2010); however, the response of IRF9 to I/R is not clear. Cerebral ischemia induced by MCAO closely mimics the pathologies observed during human stroke (Engel et al., 2011). To study the biological impact of IRF9 on ischemic stroke, we first examined the expression pattern of IRF9 in a mouse model of stroke. In response to MCAO/reperfusion (MCAO for 45 min followed by reperfusion for 72 h after the stroke onset), IRF9 expression increased in brain homogenates in a time-dependent manner. IRF9 was induced as early as 2 h after MCAO and further increased by ~2.7-fold of its normal expression level in the brain by 72 h (Fig. 1*A*). Neurons are at particular risk of ischemic injury due to their high energy demand (Tymianski, 2011). IRF9 was expressed at low levels in the contralateral (control) cortex (Fig. 1*B*,*C*). However, when the ipsilateral cortex was subjected to MCAO/reperfusion *in vivo*, heavy IRF9 staining was observed. This pattern of IRF9 was coexpressed with neuron-specific nuclear protein (NeuN) (Fig. 1*B*) and microtubule-associated protein-2 (MAP2) (Fig. 1*C*). Importantly, IRF9 aggregated in both cortical and striatal neurons but not in the hippocampus (Fig. 1*D*), where cerebral blood flow was not compromised by MCAO (Engel et al., 2011). Therefore, IRF9

←

Figure 3. IRF9 increases neuronal death in ischemic models *in vitro* and *in vivo*. ***A–D***, Cell viability (***A***, ***C***) and LDH release (***B***, ***D***) were assessed and quantified after OGD at the indicated time points. The primary neurons were infected with AdshIRF9 (***A***, ***B***), AdIRF9 (***C***, ***D***), or control adenoviruses. $n = 9$ per time point. ***A***, ***B***, $^{*}p < 0.05$ compared with AdshRNA. ***C***, ***D***, $^{*}p < 0.05$ compared with AdGFP. ***E***, The cortices from the indicated mouse lines were stained with Fluoro-Jade B, TUNEL, and DAPI (blue) 24 h after I/R. ***F***, Fluoro-Jade B- and TUNEL-positive neurons were quantified. $n = 3$–5. $^{*}p < 0.05$ versus WT (left) or NTG (right) mice. ***G***, Brain sections from IRF9-KO and -TG mice were stained for cleaved caspase-3 (green) and DAPI (blue) after 24 h I/R. Bottom, Cleaved caspase-3-positive neurons were quantified. $n = 3$ or 4. $^{*}p < 0.05$ versus control mice. ***H–K***, Western blotting of the indicated proteins in brain homogenates from sham- and MCAO-operated IRF9-KO (***H***) and IRF9-TG (***I***) mice or cell lysates from AdshIRF9- (***J***) and AdIRF9-infected (***K***) primary neurons. GAPDH served as a loading control. Right panels, Densitometric analysis of the normalized protein levels. $n = 3$–6. $^{*}p < 0.05$ versus sham (***H***, ***I***) or AdshRNA (***J***), or AdGFP (***K***). ***H***, $^{\#}p < 0.05$ versus WT. ***I***, $^{\#}p < 0.05$ versus NTG. Error bars indicate mean ± SE. Scale bars: ***E***, ***G***, 20 μm. ***L***, ***M***, Western blotting of the cytochrome *c*, COX2, and LDH in cytosol (top) or mitochondria (bottom) in brain homogenates from sham- and MCAO-operated IRF9-KO (***L***) and IRF9-TG (***M***) mice. $n = 3$. $^{*}p < 0.05$ versus control. Error bars indicate mean ± SE.

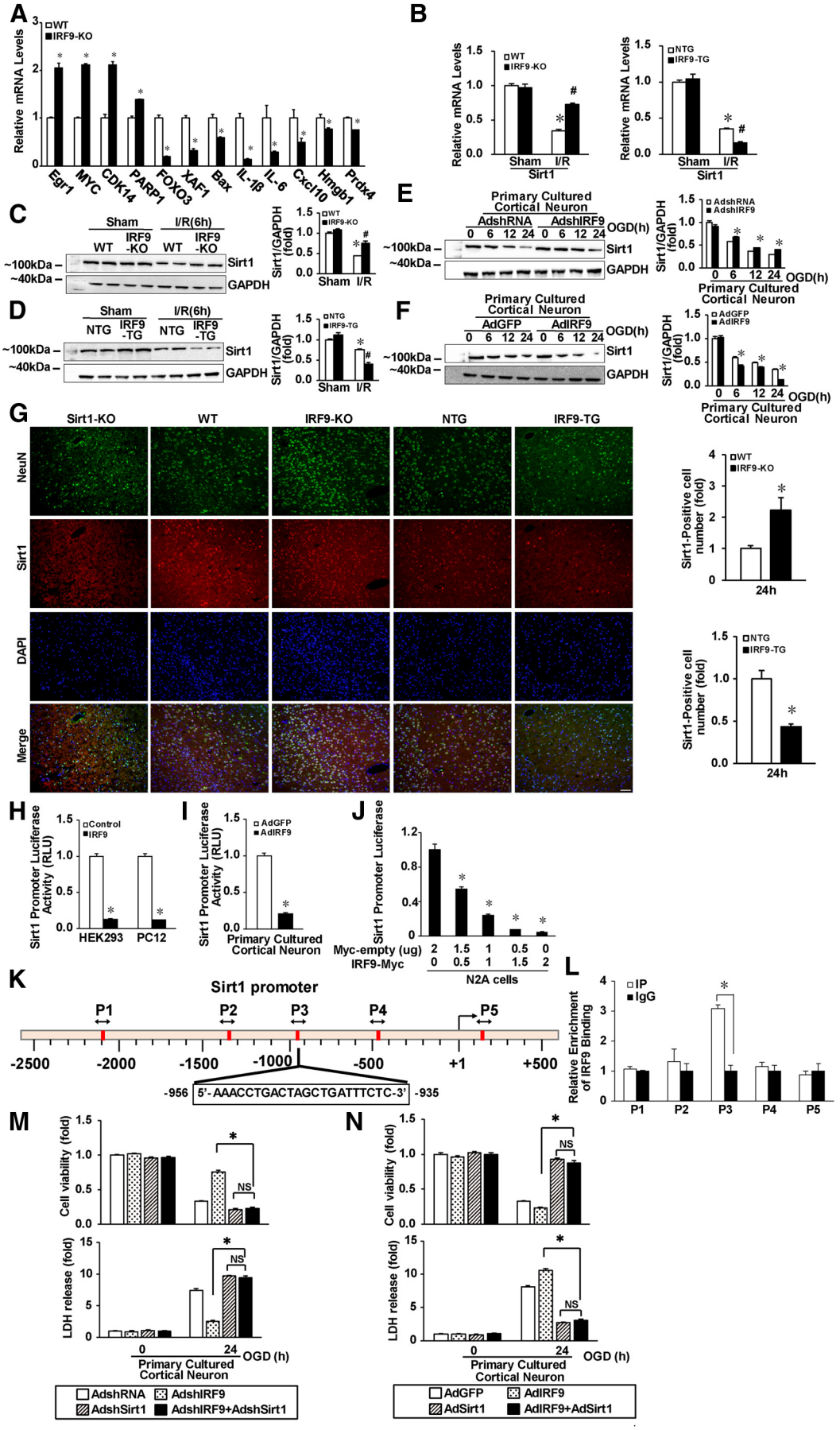
A
WT
IRF9-KO
Relative mRNA Levels
Egr1
MYC
CDK14
PARP1
FOXO3
XAF1
Bax
IL-1β
IL-6
Cxcl10
Hmgb1
Prdx4
B
WT
IRF9-KO
Relative mRNA Levels
Sham
I/R
Sirt1
NTG
IRF9-TG
C
Sham
I/R(6h)
WT
IRF9 -KO
~100kDa
~40kDa
Sirt1
GAPDH
Sirt1/GAPDH (fold)
D
NTG
IRF9 -TG
E
Primary Cultured Cortical Neuron
AdshRNA
AdshIRF9
OGD(h)
0 6 12 24
F
AdGFP
AdIRF9
G
Sirt1-KO
WT
IRF9-KO
NTG
IRF9-TG
NeuN
Sirt1
DAPI
Merge
Sirt1-Positive cell number (fold)
24h
H
Control
IRF9
Sirt1 Promoter Luciferase Activity (RLU)
HEK293
PC12
I
AdGFP
AdIRF9
Primary Cultured Cortical Neuron
J
Sirt1 Promoter Luciferase
Myc-empty (ug)
IRF9-Myc
N2A cells
K
Sirt1 promoter
P1
P2
P3
P4
P5
-2500
-2000
-1500
-1000
-500
+1
+500
-956
5'- AAACCTGACTAGCTGATTTCTC-3'
-935
L
IP
IgG
Relative Enrichment of IRF9 Binding
M
Cell viability (fold)
LDH release (fold)
NS
OGD (h)
AdshRNA
AdshIRF9
AdshSirt1
AdshIRF9+AdshSirt1
N
AdGFP
AdIRF9
AdSirt1
AdIRF9+AdSirt1

is specifically induced in neurons upon I/R insult. To rule out potential systemic or inflammatory interference, rat primary cortical neurons were isolated and challenged with OGD for 1 h, followed by normal culture conditions for the indicated time periods (Fig. 1*E*). Neurons subjected to OGD displayed a time-dependent increase in the expression of IRF9 *in vitro*, as shown by immunostaining (Fig. 1*F*) and Western blot analyses (Fig. 1*G*). Next, we sought to determine the potential clinical significance of these observations in human samples. Considering that it was almost impossible to obtain samples from ischemic stroke patients, we examined the expression of IRF9 in normal and intracerebral hemorrhagic human brains. ICH leads to significant neuronal loss after blood entry. To a certain extent, this effect mimics the detrimental cerebral injury and neuronal death in ischemic stroke. Interestingly, we found that ICH increases IRF9 protein expression by ~1.6-fold (Fig. 1*H*). Together, these data indicate that IRF9 in neurons may play a functional role in stroke pathology in both mice and humans.

IRF9 exacerbates poststroke cerebral injury

Considering that neuronal IRF9 is robustly induced by I/R, we investigated whether a forced overexpression of IRF9 in neurons would contribute to I/R-induced cerebral injury. IRF9-TG were generated by crossing $Irf9^{flox/flox}$ mice with mice carrying a Cre recombinase driven by the neuron-specific promoter *CaMKIIα* (Fig. 2*A*). *IRF9*-TG3 (hereafter referred to as *IRF9*-TG) mice displayed a 4.27-fold increase in cerebral IRF9 expression (Fig. 2*B*), which is similar to the increase observed in mice during stroke. Because of the profound effects of blood pressure and heart rate on stroke outcome, we first examined these parameters in NTG and *IRF9*-TG mice before MCAO (Table 1). No significant differences were observed between the two mouse strains, and IRF9 overexpression in neurons did not compromise vascular integrity (Fig. 2*D*). In addition, both NTG and *IRF9*-TG mice underwent comparable regional cerebral blood flow (rCBF) perfusion during the course of I/R (Fig. 2*F*). Compared with the NTG mice, the *IRF9*-TG mice exhibited an increase in infarct volume of ~128.45% and 72.77% at 24 and 72 h after MCAO, respectively (Fig. 2*G*,*H*). Functionally, IRF9-TG mice exhibited exacerbated neurological deficits at both time points (47.37% increase at 24 h and 38.66% increase at 72 h) (Fig. 2*I*). In live *IRF9*-TG mice, the lesion size was also larger at 24 h than that observed in the NTG mice, as shown by imaging (Fig. 2*J*) and as evaluated by MRI (Fig. 2*K*). Thus, the induction of IRF9 in neurons evidently contributes to the progression of cerebral lesions after I/R.

Next, we assessed whether IRF9 upregulation is required for ischemic cerebral damage. *IRF9* ablation had no impact on blood pressure, heart rate, vascular integrity, or rCBF (Table 1; Fig. 2*C*,*E*). However, *IRF9*-KO mice that were challenged with I/R for 24 h, 72 h, or 7 d had significantly improved stroke outcomes compared with WT mice, both histologically (Fig. 2*L*,*M*) and functionally (Fig. 2*N*). This cerebroprotective effect of *IRF9* ablation was confirmed by MRI in live mice (Fig. 2*O*,*P*). Moreover, we investigated whether IRF9 targeted other cell types in the CNS, namely, astrocytes and microglia. Astrocyte- (*GFAP-Cre/IRF9*-TG) and microglia-specific IRF9-overexpressing transgenic (*Lyz-Cre/IRF9*-TG) mice were generated. After I/R, both transgenic mouse lines showed a similar infarct volume and neurological deficits compared with their control littermates (Fig. 2*Q*,*R*). Collectively, these findings unambiguously demonstrate that IRF9 mediates ischemic brain damage by directly targeting neurons.

IRF9 potentiates postischemic neuronal death

Given that neuronal IRF9 is specifically induced by I/R and that neuron-specific IRF9 sufficiently potentiates cerebral injury, we investigated whether IRF9 exerts a direct effect on neuronal survival. Therefore, we infected rat primary cortical neurons with either *AdshIRF9*, which reduced IRF9 expression by >90% (data not shown), or its scrambled control, *AdshRNA*. Indeed, the *IRF9*-silenced neurons were more resistant to OGD-induced cell death, as evidenced by their significantly enhanced cell viability and reduced LDH release (Fig. 3*A*,*B*); conversely, IRF9 overexpression (*Ad-IRF9*) rendered the neurons more vulnerable to OGD-induced cell death (Fig. 3*C*,*D*).

Necrosis and apoptosis are fundamental mechanisms of the cell death that ensues after stroke. Because IRF9 continues to be involved in ischemic injury even 7 d after stroke onset, we hypothesized that IRF9 may exert a more prominent effect on delayed neuronal death. To test this hypothesis, we next performed Fluoro-Jade B TUNEL staining in *IRF9*-KO and *IRF9*-TG mice 24 h after MCAO (Fig. 3*E*). Fluoro-Jade B is a specific marker for acutely degenerating neurons, regardless of the cause of death (Schmued and Hopkins, 2000). *IRF9* ablation reduced the number of Fluoro-Jade B-positive cells by ~78.73% and TUNEL-positive cells by >90%. By contrast, Fluoro-Jade B-positive cells and TUNEL-positive cells were increased by 1.04-fold and 1.72-fold, respectively, in *IRF9*-TG mice (Fig. 3*F*). Thus, IRF9 is critical for I/R-induced neuronal degeneration and apoptosis. The proapoptotic effect of IRF9 was further confirmed by immunostaining of cleaved caspase-3 *in vivo* (Fig. 3*G*). Western blot analysis showed that the expression of the antiapoptotic protein Bcl2 was decreased and the expression levels of the proapoptotic protein cleaved caspase3 were increased in WT and NTG mice at 6 h after I/R compared with sham controls (Fig. 3*H*,*I*); however, these changes were significantly attenuated in *IRF9*-KO mice (Fig. 3*H*) and enhanced in *IRF9*-TG mice compared with WT and NTG mice, respectively (Fig. 3*I*). These results suggest a critical role for IRF9 in neuronal apoptosis. Moreover, the temporal expression patterns of these proteins were similar in OGD-treated primary neuronal cells infected with AdshIRF9 (Fig. 3*J*) or *Ad-IRF9* (Fig. 3*K*). To establish a causal link between IRF9 and caspase-3 activation, we further investigated whether IRF9 promoted cytochrome *c* release. In response to I/R, cytochrome *c* was released from mitochondria into the cytoplasm. However, IRF9 knock-out significantly repressed this release (Fig. 3*L*), whereas

←

Figure 4. IRF9 inhibits *Sirt1* transcription. ***A***, The mRNAs of Sirt1-regulated genes were detected by RT-PCR in six independent experiments. $*p < 0.05$ versus WT mice. ***B***, *Sirt1* mRNA in sham- or MCAO-operated mice of the indicated genotypes. $*p < 0.05$ versus sham; $\#p < 0.05$ versus WT or NTG mice. ***C–F***, Immunoblotting of Sirt1 in brain homogenates from sham- and MCAO-operated IRF9-KO (***C***) and IRF9-TG (***D***) mice or cell lysates from AdshIRF9- (***E***) and AdIRF9-infected (***F***) primary neurons. GAPDH served as a loading control. Right panels, Densitometric analysis of the normalized protein levels. $n = 3–6$. $*p < 0.05$ versus sham (***C***, ***D***), AdshRNA (***E***), or AdGFP (***F***). $^{\#}p < 0.05$ versus WT (***C***) or NTGmice (***D***). ***G***, Cortices from the indicated genotypes were stained for NeuN, Sirt1, and DAPI (blue) after 24 h I/R. Quantification of Sirt1-positive neurons in 3 or 4 independent experiments is shown. $*p < 0.05$ versus control. ***H***, ***I***, Sirt1 promoter luciferase activity was assessed in controls, IRF9-overexpressing cell lines (***H***) and primary neurons (***I***). $*p < 0.05$ versus control. ***J***, Sirt1 promoter luciferase activity was assessed in controls and IRF9-overexpressing N2A cell lines with the indicated dose. $n = 9$. $*p < 0.05$ versus control. ***K***, Schematic of the Sirt1 promoter construct containing 5 putative IRF9 binding sites (P1-P5). ***L***, IRF9 was enriched in the P3 region, as shown by ChIP. $n = 5$. $*p < 0.05$ versus IP controls. ***M***, ***N***, Cell viability and LDH release before or after 24 h of OGD were assessed in primary neurons infected with the indicated adenoviruses and quantified. $n = 9$ per time point. $*p < 0.05$ compared with AdshIRF9 (***M***) or AdIRF9 (***N***). NS, Not significant. Error bars indicate mean ± SE.

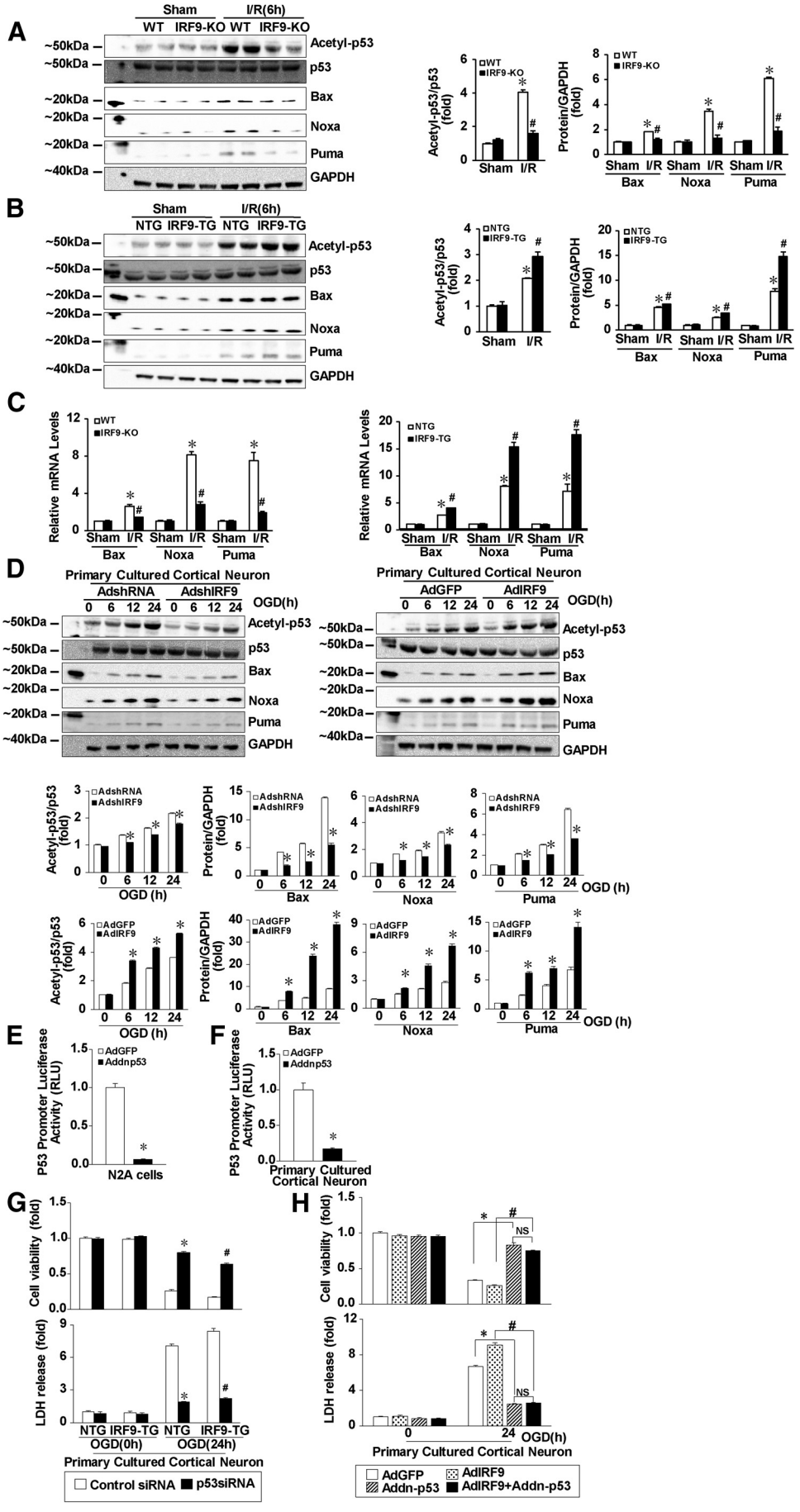
A
Sham
I/R(6h)
WT IRF9-KO WT IRF9-KO
~50kDa
Acetyl-p53
p53
~20kDa
Bax
Noxa
Puma
~40kDa
GAPDH
Acetyl-p53/p53 (fold)
Protein/GAPDH (fold)
WT
IRF9-KO
Sham I/R
Bax Noxa Puma
B
NTG IRF9-TG NTG IRF9-TG
C
Relative mRNA Levels
D
Primary Cultured Cortical Neuron
AdshRNA AdshIRF9
OGD(h)
0 6 12 24
AdGFP AdIRF9
OGD (h)
E
P53 Promoter Luciferase Activity (RLU)
AdGFP
Addnp53
N2A cells
F
Primary Cultured Cortical Neuron
G
Cell viability (fold)
LDH release (fold)
NTG IRF9-TG NTG IRF9-TG
OGD(0h) OGD(24h)
Control siRNA p53siRNA
H
NS
0 24 OGD(h)
AdGFP AdIRF9
Addn-p53 AdIRF9+Addn-p53

IRF9 overexpression facilitated this biological process (Fig. 3*M*). Together, these data indicate that IRF9 accelerates neuronal apoptosis in response to stroke insult.

IRF9 downregulates Sirt1 expression

To investigate the regulatory mechanism of IRF9 in response to I/R insults, penumbra tissues were harvested from WT and *IRF9*-KO mice after 24 h of MCAO/reperfusion. Next, mRNAs were extracted from these tissues and screened using a genome-wide mRNA array. It was determined that the mRNA levels of a dozen genes involved in ischemic injury, including *Egr1*, *MYC*, and *FOXO3*, were significantly altered in *IRF9*-KO mice compared with WT controls (Table 2; Fig. 4*A*). Intriguingly, these genes are regulated by the deacetylase Sirt1, a putative prosurvival gene that protects against poststroke cerebral injury (Liu et al., 2009; Hernández-Jiménez et al., 2013). Using real-time PCR, we observed that Sirt1 mRNA levels were also upregulated by >2-fold in *IRF9*-KO mice (Fig. 4*B*).

To further explore these findings, we examined the effects of manipulating the IRF9 expression level on cerebral Sirt1 protein expression. Western blot analysis showed that an increase in IRF9 protein expression in the poststroke penumbra was accompanied by an ~56.48% decrease in Sirt1 in WT mice (Fig. 4*C*). Nevertheless, Sirt1 expression was largely maintained in *IRF9*-KO mice at a time point of 6 h after I/R (Fig. 4*C*). By contrast, the overexpression of IRF9 in neurons led to an ~47.28% reduction in penumbral Sirt1 expression compared with NTG mice (Fig. 4*D*), indicating that IRF9 exerts an inhibitory effect on Sirt1 expression. The negative correlation between IRF9 and Sirt1 expression was further validated in primary cortical neurons *in vitro* (Fig. 4*E*,*F*). Indeed, a costaining of Sirt1 and NeuN demonstrated that, at 24 h after MCAO, the number of Sirt1-positive neurons increased by ~2-fold in *IRF9*-KO mice and decreased to <50% in *IRF9*-TG mice compared with their control littermates (Fig. 4*G*).

Given that IRF9 is a well-characterized transcription factor targeting the ISREs of downstream genes, we investigated whether the inhibitory effect of IRF9 on Sirt1 expression was attributable to IRF9-dependent transcriptional regulation. Thus, we examined *Sirt1* promoter activity in HEK293 and PC12 cell lines transfected with *IRF9* or an empty vector after OGD/reperfusion (Fig. 4*H*). The overexpression of IRF9 reduced *Sirt1* promoter luciferase activity to 13.07% and 11.99% of the controls in HEK293 and PC12 cell lines (Fig. 4*H*), respectively, as well as in primary cortical neuronal cultures infected with *Ad-IRF9* (79.40% reduction compared with *Ad-GFP*; Fig. 4*I*). Intriguingly, overexpressing IRF9, but not its scrambled controls, inhibited the luciferase activity of Sirt1-Luc in N2A cells in a dose-dependent manner (Fig. 4*J*). Next, we performed a ChIP assay of IRF9 followed by quantitative PCR of the murine *Sirt1* promoter (Fig. 4*K*). Using bioinformatics approaches, a series of putative ISRE binding sites, designated P1-P5, were identified (Fig. 4*K*). To increase the specificity of the ChIP analysis, only sequences containing at least two ISRE repeats (5′-GAAA-3′) were considered as potential IRF9 binding sites. We observed that IRF9 ChIPs were enriched for the P3 region but not any of the other regions, indicating that P3 contains the primary site for IRF9 binding (Fig. 4*K*,*L*). To assess whether the inhibition of Sirt1 expression is necessary for IRF9-mediated neuronal apoptosis, we infected primary cortical neurons with *AdshIRF9*, *AdshSirt1*, or both *AdshIRF9* and *AdshSirt1* (Fig. 4*M*). Coinfection with *AdshSirt1* completely abolished the neuroprotective effect of *IRF9* ablation (Fig. 4*M*). Conversely, IRF9-mediated neuronal death was reversed by infection with adenovirus overexpressing Sirt1 (*AdSirt1*) (Fig. 4*N*). These data show that, during ischemic stroke, the upregulation of IRF9 negatively regulates *Sirt1* transcription, thereby inhibiting Sirt1 expression and eventually culminating in neuronal death.

IRF9 increases p53 acetylation and activation

p53, a critical transcriptional activator that controls apoptotic programs, was the first nonhistone deacetylation target identified for Sirt1 (Luo et al., 2001; Vaziri et al., 2001). Hasegawa and Yoshikawa (2008) recently reported that p53-induced DNA damage can be reduced via Sirt1-mediated p53 deacetylation in cortical neurons. In addition, Raz et al. (2011) showed that global cerebral ischemia enhanced p53 acetylation in the hippocampal CA1 region. Thus, we hypothesized that the IRF9-Sirt1 axis may regulate neuronal death through p53-dependent apoptotic programs. To test this hypothesis experimentally, we examined the effect of IRF9 on p53 acetylation. At 6 h after I/R in WT mice, p53 became acetylated, and the expression of myriad of p53-dependent proapoptotic proteins, including Bax, Noxa, and Puma, to name just a few, increased (Fig. 5*A*,*B*). By contrast, *IRF9*-KO caused a significant decrease in the expression of acetyl-p53, Bax, Noxa, and Puma compared with WT mice in the setting of ischemic stroke (Fig. 5*A*), an effect that was reversed by the neuron-specific overexpression of IRF9 *in vivo* (Fig. 5*B*). Importantly, the total p53 expression level was not altered by *IRF9* gene manipulation (Fig. 5*A*,*B*). IRF9 also positively regulated the mRNA levels of *Bax*, *Noxa*, and *Puma* (Fig. 5*C*), suggesting that IRF9 facilitates both the acetylation of p53 and *p53* transactivation. The activation of p53 apoptotic programs was further confirmed in a complementary *in vitro* experiment (Fig. 5*D*). Next, we assessed whether p53 is essential for IRF9-mediated neuronal death. Small interfering RNA (siRNA) knockdown of *p53* (*p53siRNA*) reduced p53 expression to <35% of controls (data not shown), whereas *Addnp53*, an adenovirus harboring a dominant-negative form of p53, reduced p53 activity to ~6.41% and 16.50% in N2A cells and primary cortical neurons, respectively (Fig. 5*E*,*F*). *p53siRNA* largely reversed OGD-induced cell death in the primary neurons isolated from NTG and *IRF9*-TG mice (Fig. 5*G*). Furthermore, *AdIRF9*-mediated neuronal death was completely abolished when the cells were coinfected with Addn-p53 (Fig. 5*H*). Thus, p53 is suggested to be a major downstream effector of the IRF9 signaling pathway. Together, these data demonstrate that IRF9-induced neuronal death is mediated by the acetylation and transactivation of p53.

←

Figure 5. IRF9 facilitates p53 acetylation and activation through Sirt1 inhibition. Western blotting and quantification of the indicated p53 pathway proteins isolated from IRF9-KO (***A***) and IRF9-TG mice (***B***) before I/R and 6 h after I/R. ***C***, The mRNAs of p53-regulated genes were detected by RT-PCR in four independent experiments. $^{*}p < 0.05$ versus sham controls. $^{\#}p < 0.05$ versus MCAO-operated WT or NTG. ***D***, Western blotting and densitometric analysis of the proteins in the p53 pathway in OGD-treated primary neurons infected with the indicated adenoviruses. $^{*}p < 0.05$ versus AdGFP or AdshRNA controls. ***E***, ***F***, p53 promoter luciferase activity was assessed in controls and Addnp53-infected N2A cell lines (***E***) and primary cortical neurons (***F***). $n = 9$. $^{*}p < 0.05$ versus AdGFP controls. ***G***, ***H***, Cell viability and LDH release after OGD at the indicated time points were assessed and quantified in primary neurons isolated from IRF9-TG mice (***G***) or rat (***H***). The primary neurons were infected with the indicated adenoviruses. $n = 3$ or 4. $^{*}p < 0.05$ compared with siRNA (***G***) or AdGFP (***H***). $^{\#}p < 0.05$ versus NTG (***G***) or AdIRF9 (***H***). NS, Not significant. Error bars indicate mean ± SE.

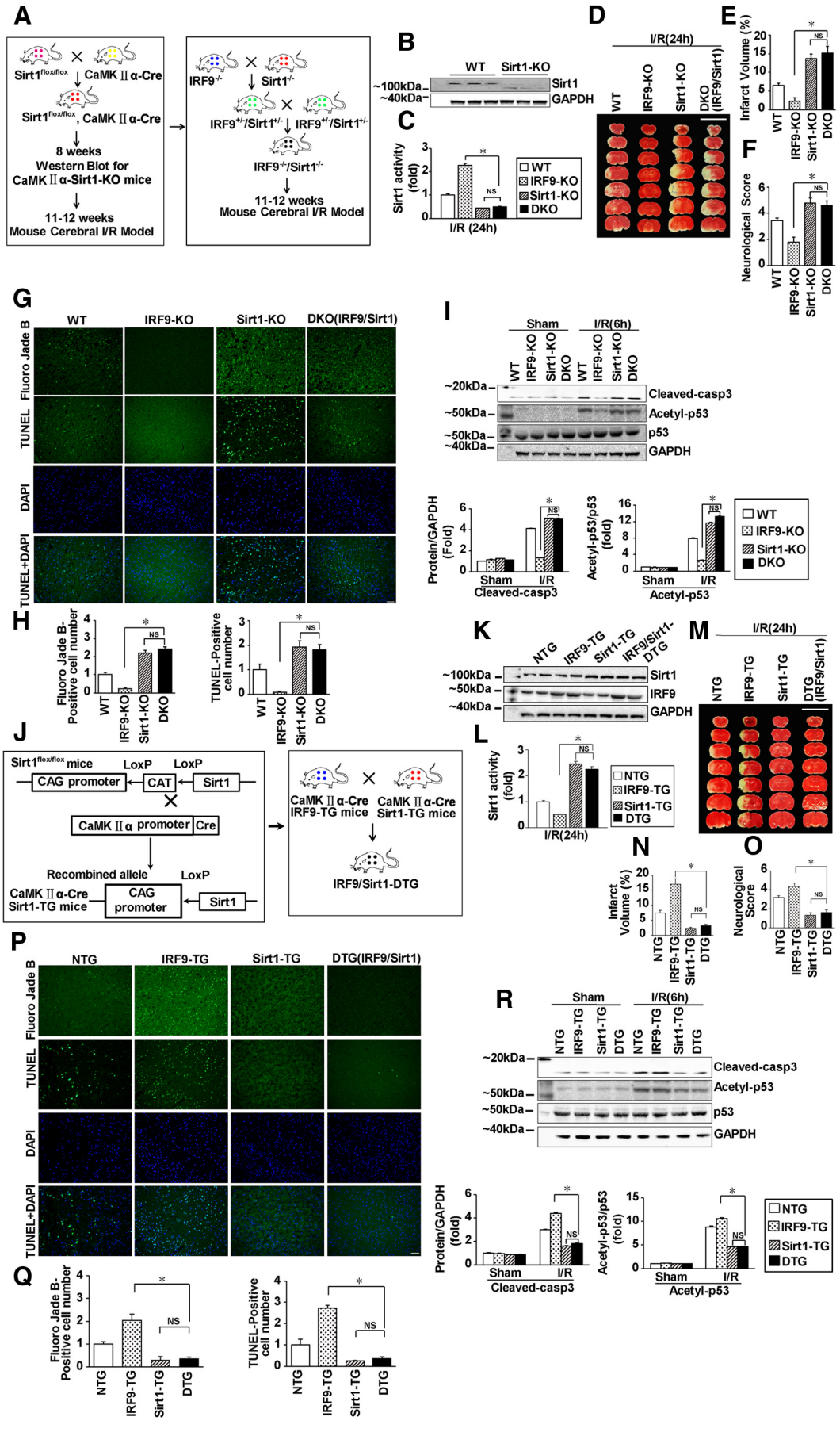
A
Sirt1flox/flox × CaMKIIα-Cre
Sirt1flox/flox, CaMKIIα-Cre
8 weeks
Western Blot for CaMKIIα-Sirt1-KO mice
11-12 weeks
Mouse Cerebral I/R Model
IRF9-/- × Sirt1-/-
IRF9+/-/Sirt1+/- × IRF9+/-/Sirt1+/-
IRF9-/-/Sirt1-/-
11-12 weeks
Mouse Cerebral I/R Model
B
WT Sirt1-KO
~100kDa Sirt1
~40kDa GAPDH
C
Sirt1 activity (fold)
I/R (24h)
WT
IRF9-KO
Sirt1-KO
DKO
D
I/R(24h)
WT IRF9-KO Sirt1-KO DKO (IRF9/Sirt1)
E
Infarct Volume (%)
F
Neurological Score
G
WT IRF9-KO Sirt1-KO DKO(IRF9/Sirt1)
Fluoro Jade B
TUNEL
DAPI
TUNEL+DAPI
H
Fluoro Jade B-Positive cell number
TUNEL-Positive cell number
I
Sham I/R(6h)
~20kDa Cleaved-casp3
~50kDa Acetyl-p53
~50kDa p53
~40kDa GAPDH
Protein/GAPDH (Fold)
Cleaved-casp3
Acetyl-p53/p53 (fold)
Acetyl-p53
J
Sirt1flox/flox mice
LoxP CAT LoxP
CAG promoter
Sirt1
CaMKIIα promoter Cre
Recombined allele
CaMKIIα-Cre Sirt1-TG mice
CaMKIIα-Cre IRF9-TG mice × CaMKIIα-Cre Sirt1-TG mice
IRF9/Sirt1-DTG
K
NTG IRF9-TG Sirt1-TG IRF9/Sirt1-DTG
~100kDa Sirt1
~50kDa IRF9
~40kDa GAPDH
L
Sirt1 activity (fold)
I/R(24h)
NTG
IRF9-TG
Sirt1-TG
DTG
M
I/R(24h)
NTG IRF9-TG Sirt1-TG DTG (IRF9/Sirt1)
N
Infarct Volume (%)
O
Neurological Score
P
NTG IRF9-TG Sirt1-TG DTG(IRF9/Sirt1)
Fluoro Jade B
TUNEL
DAPI
TUNEL+DAPI
Q
Fluoro Jade B-Positive cell number
TUNEL-Positive cell number
R
Sham I/R(6h)
~20kDa Cleaved-casp3
~50kDa Acetyl-p53
~50kDa p53
~40kDa GAPDH
Protein/GAPDH (fold)
Cleaved-casp3
Acetyl-p53/p53 (fold)
Acetyl-p53

Sirt1 is required for IRF9/p53-mediated ischemic neuronal death

Having established that IRF9 inhibits Sirt1 transcription and that IRF9 mediates p53 acetylation and transactivation, we examined whether the IRF9-p53 axis relies on Sirt1 expression *in vivo*. *IRF9*-KO mice were crossed with *Sirt1*-KO mice to generate DKO (Fig. 6*A*,*B*). Notably, Sirt1 deacetylase activity was not significantly different between the *Sirt1*-KO and DKO mice (Fig. 6*C*). Importantly, we observed that stroke outcomes were exacerbated in the DKO mice compared with the IRF9-KO mice but were comparable in the *Sirt1*-KO and DKO mice (Fig. 6*D–F*). Accordingly, *IRF9*-KO-mediated neuronal survival, decreased p53 acetylation, and neuronal apoptosis were all abrogated in the DKO mice (Fig. 6*G–I*).

To further examine the relationship between the IRF9-Sirt1 axis and p53-dependent apoptotic programs, we crossed *IRF9*-TG mice with neuron-specific *Sirt1* transgenic (*Sirt1*-TG) mice to generate DTG mice (Fig. 6*J*), which we validated by Western blotting (Fig. 6*K*). Decreased Sirt1 activity in the *IRF9*-TG mice was fully restored in the DTG mice to a level comparable with the *Sirt1*-TG mice (Fig. 6*L*). DTG mice showed a substantial amelioration of deteriorated stroke outcomes (Fig. 6*M–O*), neuronal survival (Fig. 6*P*,*Q*), and inhibited p53 apoptotic programs (Fig. 6*R*) compared with the *IRF9*-TG mice. Similar to the results obtained with the KO mice, these results were comparable between the *Sirt1*-TG and DTG mice (Fig. 6*L–R*). Based on these data, we conclude that Sirt1 is required for IRF9-mediated p53 acetylation and neuronal death.

IRF9-mediated cerebral injury is dependent on Sirt1 deacetylase activity

Finally, considering that Sirt1 is a well-recognized deacetylase, we investigated whether Sirt1 deacetylase activity was responsible for the IRF9-mediated effects of stroke. After I/R, Sirt1 activity was negatively correlated with IRF9 expression both *in vivo* (Fig. 7*A*) and *in vitro* (Fig. 7*B*). Indeed, the overexpression of a Sirt1 deacetylase mutant (H363Y) failed to rescue neurons from IRF9-mediated death (Fig. 7*C*). Next, we treated neuronal cultures with the Sirt1 inhibitors nicotinamide and EX527 or with the Sirt1 activators resveratrol and SRT1720 before subjecting them to OGD/reperfusion (Fig. 7*D*,*E*). Cell survival assays indicated that Sirt1 activity was both sufficient and necessary for the IRF9-mediated neuronal death. To further examine this phenomenon *in vivo*, we intracranially injected either EX527 or SRT1720 into *IRF9*-KO or *IRF9*-TG mice, respectively, before challenging the mice with MCAO/reperfusion. EX527, a Sirt1-specific inhibitor, diminished Sirt1 activity in the neurons derived from *IRF9*-KO mice; conversely, SRT1720 specifically activated Sirt1 activity upon IRF9 overexpression (Fig. 7*F*). Importantly, the intracranial injection of EX527 or SRT1720 into *IRF9*-KO mice or *IRF9*-TG mice, respectively, recapitulated our observations in the *IRF9*/*Sirt1*-DKO or -DTG mice with respect to stroke outcome (Fig. 7*G*,*H*), neuronal death (Fig. 7*I*,*J*), and p53 signaling (Fig. 7*K*,*L*). Together, these findings indicate that IRF9 is a previously unrecognized negative regulator of the Sirt1/p53 axis. Furthermore, our results show that the IRF9-Sirt1-p53 axis is functionally necessary for ischemic cerebral injury.

←

Figure 6. Generation of IRF9/Sirt1 DKO and DTG mice; IRF9-mediated neuronal death is Sirt1 dependent; Sirt1 mediates IRF9-induced p53 activation and neuronal death. ***A***, Generation of neuron-specific IRF9/Sirt1 DKO mice. ***B***, A representative Western blot of Sirt1 in WT and Sirt1-KO mice. GAPDH served as a loading control. ***C***, Sirt1 deacetylase activity was assessed in the brains of WT, IRF9-KO, Sirt1-KO, and DKO mice at 24 h after I/R. $n = 9$. $^*p < 0.05$ versus IRF9-KO mice. ***D***, TTC-stained sections from WT, IRF9-KO, Sirt1-KO, and DKO mice at 24 h after I/R. ***E***, ***F***, Quantification of infarct volumes (***E***) and neurological deficit scores (***F***) 24 h after I/R. $n = 5–7$. $^*p < 0.05$ versus IRF9-KO mice. ***G***, Representative images of the cortices from the indicated mouse lines stained with Fluoro-Jade B, TUNEL, and DAPI (blue) 24 h after I/R. ***H***, Quantification of Fluoro Jade B- and TUNEL-positive neurons in the indicated genotypes. $n = 3$ or 4. $^*p < 0.05$ versus IRF9-KO mice. ***I***, Western blotting and quantification of cleaved caspase-3, acetyl-p53, and total p53 in the indicated genotypes. $^*p < 0.05$ versus IRF9-KO mice. ***J***, Generation of IRF9/Sirt1 DTG mice. ***K***, A representative Western blot of Sirt1 and IRF9 in DTG mice. GAPDH served as a loading control. ***L***, Sirt1 deacetylase activity was assessed in the brains of NTG, IRF9-TG, Sirt1-TG, and DTG mice at 24 h after I/R. $n = 9$. $^*p < 0.05$ versus IRF9-TG mice. ***M***, TTC-stained sections from NTG, IRF9-TG, Sirt1-TG, and DTG mice at 24 h after I/R. ***N***, ***O***, Quantification of infarct volumes (***N***) and neurological deficit scores (***O***) 24 h after I/R. $n = 5–8$. $^*p < 0.05$ versus IRF9-TG mice. ***P***, Representative images of the cortices from the indicated mouse lines stained with Fluoro-Jade B, TUNEL, and DAPI (blue) 24 h after I/R. ***Q***, Quantification of Fluoro Jade B- and TUNEL-positive neurons in the indicated genotypes. $n = 3–5$. $^*p < 0.05$ versus IRF9-TG mice. ***R***, Western blotting and quantification of cleaved caspase-3, acetyl-p53, and total p53 in the indicated genotypes. $^*p < 0.05$ versus IRF9-TG mice. NS, Not significant. Error bars indicate mean ± SE.

Discussion

This study demonstrates that a previously unrecognized pathway is activated upon cerebral I/R stress. I/R-induced IRF9 represses Sirt1 expression, leading to the acetylation of p53, thereby instigating neuronal death. Moreover, these results show that neuronal IRF9 is a direct mediator of brain injury after ischemia and reperfusion. Neurons are a major source of endogenous prodeath and neuroprotective regulators (Lo, 2008; Andrabi et al., 2011; Yenari and Han, 2012). Consistent with this notion, neuronal IRF9 was observed to be specifically upregulated in response to I/R. Indeed, the neuron-specific overexpression of IRF9 rendered neurons more vulnerable to I/R stress, culminating in larger infarct lesions and more severe neurological dysfunction. Conversely, *IRF9* deletion in neurons markedly mitigated both poststroke neuronal death and neurological deficits. Moreover, the deacetylase Sirt1 was found to be a novel negative transcriptional target for IRF9. IRF9 downregulated Sirt1 expression, resulting in the enhanced acetylation and activation of p53 cell-death signaling. In agreement with this finding, *IRF9*/*Sirt1*-DKO mice exhibited a similar phenotype to that observed in *Sirt1*-KO mice, whereas the detrimental effect of IRF9 overexpression observed in the *IRF9*-TG mice was completely reversed in the *IRF9*/*Sirt1*-DTG mice. Finally, the Sirt1-specific inhibitor EX527 sufficiently counteracted the beneficial effects of *IRF9* deletion on stroke; conversely, the Sirt1-specific activator SRT1720 ameliorated the enhanced I/R injury in *IRF9*-TG mice. Notably, we also used human ICH samples to investigate the effect of IRF9 on acute cerebrovascular injuries in humans due to the difficulty of obtaining human ischemic stroke samples. Indeed, studies on human patients should be particularly cautious. However, the induction of IRF9 in the ICH samples, at least in part, indicated a potential clinical significance of IRF9 upregulation during I/R, as apoptosis was also detected in the perihematomal zone in human brains. Thus, we will focus on the translation of the IRF9-Sirt1-p53 pathway into clinical therapeutic approaches in future studies.

Sirt1 is the closest mammalian homolog of yeast Sir2, a nicotinamide adenine dinucleotide-dependent histone deacetylase (Imai et al., 2000). In addition to histones, Sirt1 deacetylates a large number of transcription factors that are involved in diverse biological processes (Luo et al., 2001; Chen et al., 2005). Most studies characterize Sirt1 as a survival factor that protects against aging-associated pathologies, including cardiovascular disease, metabolic disorders, oncogenesis, and, importantly, neurode-

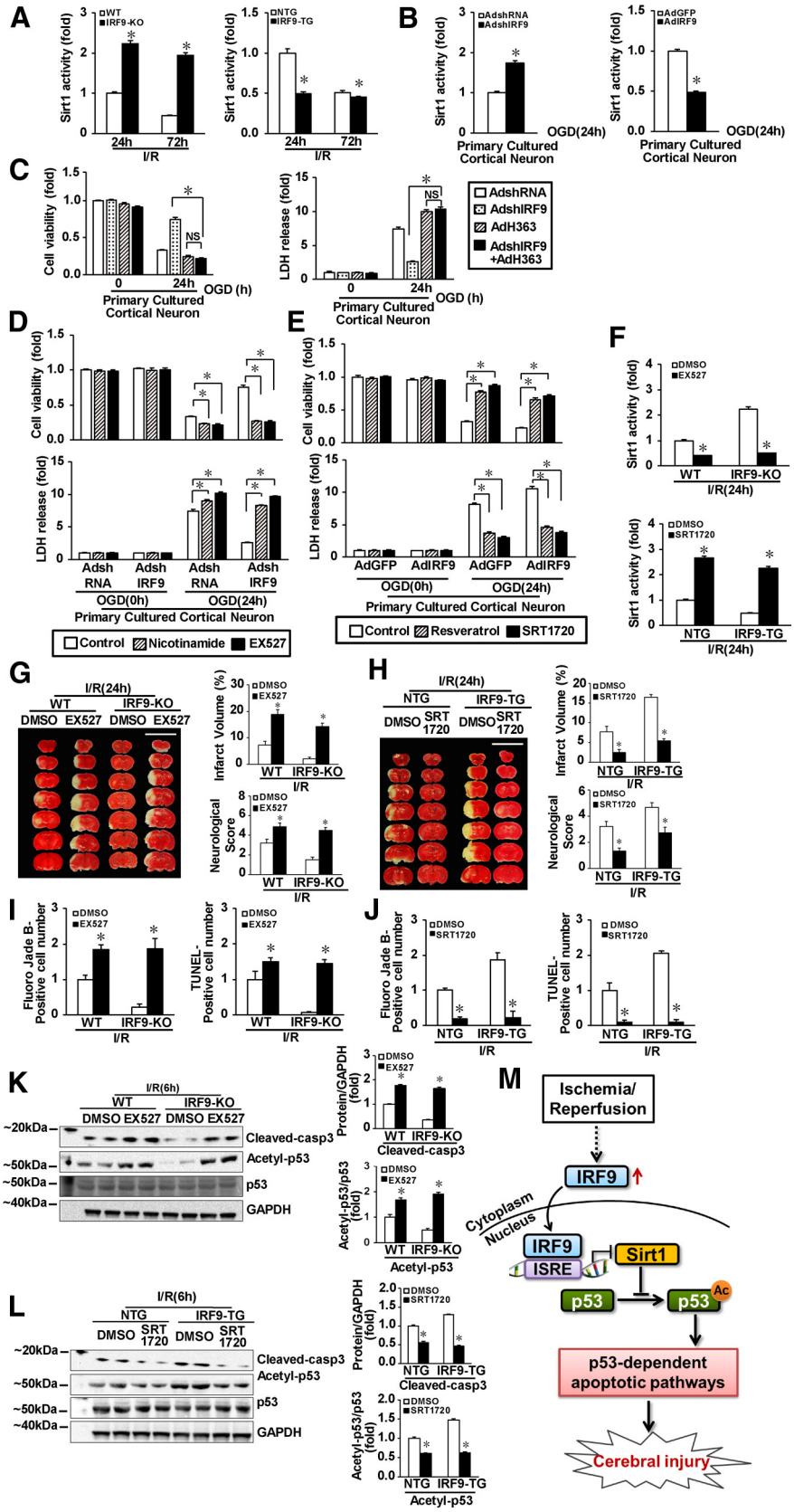

Figure 7. Sirt1 deacetylase activity is essential for IRF9-mediated ischemic injury. ***A***, ***B***, The effects of IRF9 gene manipulation on Sirt1 deacetylase activity were assessed *in vivo* (***A***) and *in vitro* (***B***). *$p < 0.05$ versus control mice (***A***) or control adenoviruses. ***C–E***, IRF9-mediated neuronal death is dependent on Sirt1 deacetylase activity, as determined by cell viability and LDH release in primary neurons lacking IRF9 (AdshIRF9) with mutated Sirt1 deacetylase activity (AdH363) (***C***). *$p < 0.05$ versus control. Neuronal survival was assessed in OGD-treated primary neuronal cultures infected with AdshIRF9 or AdIRF9 and/or the indicated Sirt1 inhibitors (***D***) and activators (***E***). ***F***, The effects of EX527 (left) and SRT1720 (right) on Sirt1 deacetylase activity in IRF9-KO and IRF9-TG mice, respectively. *$p < 0.05$ versus DMSO controls. $n = 5$. ***G***, ***H***, EX527 and SRT1720 mimic the effects of Sirt1-KO and -TG on I/R-induced cerebral injury, respectively. Representative TTC-stained sections from the indicated genotypes were quantified 24 h after I/R. *$p < 0.05$ versus DMSO (***G***, ***H***) mice. $n = 3–7$. ***I***, ***J***, Quantification of Fluoro Jade B- and TUNEL-positive neurons in the indicated genotypes. $n = 3–5$. ***K***, ***L***, Western blotting and quantification of cleaved caspase-3, acetyl-p53, and total p53 in the indicated genotypes. *$p < 0.05$ versus the DMSO group. ***M***, Proposed mechanism of IRF9 mediated I/R cerebral injury. NS, Not significant. Error bars indicate mean ± SE.

generation (Li et al., 2011; Zhou et al., 2011; Donmez, 2012; Jeong et al., 2012; Paraíso et al., 2013). Sirt1 was found to be protective against a number of neurodegenerative diseases, including Alzheimer's disease, Parkinson's disease, and Huntington's disease, through the deacetylation of either prodeath or prosurvival substrates (Kim et al., 2007; Outeiro et al., 2007; Donmez, 2012; Jeong et al., 2012; Jiang et al., 2012). Several reports have shown that Sirt1 protein expression and deacetylase activity are altered during stroke (Zhu et al., 2010; Wang et al., 2011; Hernández-Jiménez et al., 2013). Recently, Hernández-Jiménez et al. (2013) reported that Sirt1 potentiates poststroke ischemic neuronal damage in whole-body *Sirt1* KO mice. However, the underlying molecular mechanisms by which Sirt1 is regulated remain unknown. Moreover, to our knowledge, the direct neuroprotective role of Sirt1 during ischemic stroke is also undefined. Here, we demonstrate that IRF9 induction after cerebral injury leads to the suppression of Sirt1 expression and subsequent neuronal survival. Intriguingly, Sirt1 is predominantly expressed in neurons, indicating that, during I/R, the IRF9-Sirt1 axis may be neuron specific. Moreover, we showed that both Sirt1 expression and activity are essential for IRF9-mediated neuronal death. Sirt1 expression is negatively regulated by several different transcription factors, including PPARγ, HIC1, and ChREBP; however, this regulation reportedly occurs most often when the cells are energy deprived (Chen et al., 2005; Han et al., 2010; Noriega et al., 2011). Until now, little was known regarding the transcriptional modulation of Sirt1 expression under acute stress. Here, we show that IRF9 negatively regulates Sirt1 expression in response to acute I/R. In I/R-stimulated neurons, upregulated IRF9 directly binds to the ISRE region in the Sirt1 promoter. The mutation of the ISRE binding site

completely abrogated the IRF9-mediated neuronal death induced by OGD. Thus, under cerebral I/R stress, Sirt1 is a functional target of IRF9. Given the extensive roles of Sirt1 in neurological diseases, the prodeath function of IRF9 may extend to other neurodegenerative diseases in which Sirt1 exerts critical neuroprotective effects (Kim et al., 2007; Outeiro et al., 2007; Donmez, 2012; Jeong et al., 2012; Jiang et al., 2012). Collectively, our data indicate that IRF9 is a major negative regulator of neuronal survival. Furthermore, both *in vivo* and *in vitro* experiments clearly demonstrated that Sirt1 is a major downstream target of IRF9 during the course of ischemic neuronal death.

The first nonhistone substrate identified for Sirt1 was p53 (Luo et al., 2001). Sirt1 deacetylates p53 under various pathological conditions (Luo et al., 2001; Vaziri et al., 2001). Under ischemic stress, p300 interacts with p53 to facilitate p53 acetylation and coactivate p53-dependent proapoptotic genes, including Puma and Bax, leading to neuronal death. Here, we showed that p53 is necessary for IRF9-induced neuronal death. Notably, Takaoka et al. (2003) recently reported that IRF9 is required for IFN-α/β-induced p53 upregulation, and it directly binds to the ISRE of the *p53* gene. Based on our data, we cannot exclude the possibility that *p53* transcription is directly regulated by IRF9. Nonetheless, we observed that the genetic manipulation of IRF9 did not have any impact on p53 protein expression in either the MCAO or the OGD model. It is also noteworthy that p53 binds to the promoter of IRF9 in response to viral infection, thereby enhancing IRF9 protein expression (Muñoz-Fontela et al., 2008). Therefore, it is conceivable that, during I/R, IRF9-activated p53 further upregulates IRF9, consequently forming a positive feedback loop. Neuronal survival during ischemic stroke is vital for the maintenance of neurological function, which is the single most important outcome in human patients (Vosler and Chen, 2009). We demonstrated that either interference or knockdown of *p53* sufficiently counteracted the prodeath effects of IRF9 *in vitro*. Furthermore, conditional *Sirt1* overexpression blocked IRF9-mediated p53 acetylation and improved behavioral outcomes *in vivo*, supporting the notion that the IRF9/Sirt1/p53 pathway is crucial for cerebroprotection in the course of ischemic stroke.

In conclusion, we determined that the primary pathological role of IRF9 in ischemic stroke is to negatively regulate the transcription of the deacetylase Sirt1, leading to p53 acetylation and activation. To the best of our knowledge, we demonstrate here, for the first time, that acute stress other than viral infection induces IRF9 expression in neurons, a particularly vulnerable and indispensable cell type in the CNS. More importantly, the biological effects of IRF9 are linked with molecular pathways that directly initiate neuronal death and cerebral injury upon I/R stress. Considering the role of Sirt1 in neurodegenerative diseases and I/R-induced injury in other organs, interventions aimed at inhibiting IRF9 induction may be able to contribute to Sirt1-mediated cell survival.

References

Andrabi SA, Kang HC, Haince JF, Lee YI, Zhang J, Chi Z, West AB, Koehler RC, Poirier GG, Dawson TM, Dawson VL (2011) Iduna protects the brain from glutamate excitotoxicity and stroke by interfering with poly(ADP-ribose) polymer-induced cell death. Nat Med 17:692–699. CrossRef Medline

Ankarcrona M, Dypbukt JM, Bonfoco E, Zhivotovsky B, Orrenius S, Lipton SA, Nicotera P (1995) Glutamate-induced neuronal death: a succession of necrosis or apoptosis depending on mitochondrial function. Neuron 15:961–973. CrossRef Medline

Broughton BR, Reutens DC, Sobey CG (2009) Apoptotic mechanisms after cerebral ischemia. Stroke 40:e331–e339. CrossRef Medline

Chamorro Á, Meisel A, Planas AM, Urra X, van de Beek D, Veltkamp R (2012) The immunology of acute stroke. Nat Rev Neurol 8:401–410. CrossRef Medline

Chen D, Bruno J, Easlon E, Lin SJ, Cheng HL, Alt FW, Guarente L (2008) Tissue-specific regulation of SIRT1 by calorie restriction. Genes Dev 22:1753–1757. CrossRef Medline

Chen WY, Wang DH, Yen RC, Luo J, Gu W, Baylin SB (2005) Tumor suppressor HIC1 directly regulates SIRT1 to modulate p53-dependent DNA-damage responses. Cell 123:437–448. CrossRef Medline

Darnell JE Jr, Kerr IM, Stark GR (1994) Jak-STAT pathways and transcriptional activation in response to IFNs and other extracellular signaling proteins. Science 264:1415–1421. CrossRef Medline

Donmez G (2012) The neurobiology of sirtuins and their role in neurodegeneration. Trends Pharmacol Sci 33:494–501. CrossRef Medline

Engel O, Kolodziej S, Dirnagl U, Prinz V (2011) Modeling stroke in mice: middle cerebral artery occlusion with the filament model. J Vis Exp 47:2423. CrossRef Medline

Han L, Zhou R, Niu J, McNutt MA, Wang P, Tong T (2010) SIRT1 is regulated by a PPARγ-SIRT1 negative feedback loop associated with senescence. Nucleic Acids Res 38:7458–7471. CrossRef Medline

Hasegawa K, Yoshikawa K (2008) Necdin regulates p53 acetylation via Sirtuin1 to modulate DNA damage response in cortical neurons. J Neurosci 28:8772–8784. CrossRef Medline

Hernández-Jiménez M, Hurtado O, Cuartero MI, Ballesteros I, Moraga A, Pradillo JM, McBurney MW, Lizasoain I, Moro MA (2013) Silent information regulator 1 protects the brain against cerebral ischemic damage. Stroke 44:2333–2337. CrossRef Medline

Hofer MJ, Li W, Lim SL, Campbell IL (2010) The type I interferon-alpha mediates a more severe neurological disease in the absence of the canonical signaling molecule interferon regulatory factor 9. J Neurosci 30:1149–1157. CrossRef Medline

Imai S, Armstrong CM, Kaeberlein M, Guarente L (2000) Transcriptional silencing and longevity protein Sir2 is an NAD-dependent histone deacetylase. Nature 403:795–800. CrossRef Medline

Jeong H, Cohen DE, Cui L, Supinski A, Savas JN, Mazzulli JR, Yates JR 3rd, Bordone L, Guarente L, Krainc D (2012) Sirt1 mediates neuroprotection from mutant huntingtin by activation of the TORC1 and CREB transcriptional pathway. Nat Med 18:159–165. CrossRef Medline

Jiang DS, Luo YX, Zhang R, Zhang XD, Chen HZ, Zhang Y, Chen K, Zhang SM, Fan GC, Liu PP, Liu DP, Li H (2014) Interferon regulatory factor 9 protects against cardiac hypertrophy by targeting myocardin. Hypertension 63:119–127. CrossRef Medline

Jiang M, Wang J, Fu J, Du L, Jeong H, West T, Xiang L, Peng Q, Hou Z, Cai H, Seredenina T, Arbez N, Zhu S, Sommers K, Qian J, Zhang J, Mori S, Yang XW, Tamashiro KL, Aja S, et al. (2012) Neuroprotective role of Sirt1 in mammalian models of Huntington's disease through activation of multiple Sirt1 targets. Nat Med 18:153–158. CrossRef Medline

Khorooshi R, Owens T (2010) Injury-induced type I IFN signaling regulates inflammatory responses in the central nervous system. J Immunol 185:1258–1264. CrossRef Medline

Kim D, Nguyen MD, Dobbin MM, Fischer A, Sananbenesi F, Rodgers JT, Delalle I, Baur JA, Sui G, Armour SM, Puigserver P, Sinclair DA, Tsai LH (2007) SIRT1 deacetylase protects against neurodegeneration in models for Alzheimer's disease and amyotrophic lateral sclerosis. EMBO J 26:3169–3179. CrossRef Medline

Labiche LA, Grotta JC (2004) Clinical trials for cytoprotection in stroke. NeuroRx 1:46–70. CrossRef Medline

Li L, Zhang HN, Chen HZ, Gao P, Zhu LH, Li HL, Lv X, Zhang QJ, Zhang R, Wang Z, She ZG, Zhang R, Wei YS, Du GH, Liu DP, Liang CC (2011) SIRT1 acts as a modulator of neointima formation following vascular injury in mice. Circ Res 108:1180–1189. CrossRef Medline

Liu D, Gharavi R, Pitta M, Gleichmann M, Mattson MP (2009) Nicotinamide prevents NAD^+ depletion and protects neurons against excitotoxicity and cerebral ischemia: NAD^+ consumption by SIRT1 may endanger energetically compromised neurons. Neuromol Med 11:28–42. CrossRef Medline

Lo EH (2008) A new penumbra: transitioning from injury into repair after stroke. Nat Med 14:497–500. CrossRef Medline

Lo EH, Dalkara T, Moskowitz MA (2003) Mechanisms, challenges and opportunities in stroke. Nat Rev Neurosci 4:399–415. CrossRef Medline

Lu YY, Li ZZ, Jiang DS, Wang L, Zhang Y, Chen K, Zhang XF, Liu Y, Fan GC, Chen Y, Yang Q, Zhou Y, Zhang XD, Liu DP, Li H (2013) TRAF1 is a critical regulator of cerebral ischaemia-reperfusion injury and neuronal death. Nat Commun 4:2852. CrossRef Medline

Luo J, Nikolaev AY, Imai S, Chen D, Su F, Shiloh A, Guarente L, Gu W (2001) Negative control of p53 by Sir2alpha promotes cell survival under stress. Cell 107:137–148. CrossRef Medline

Moskowitz MA, Lo EH, Iadecola C (2010) The science of stroke: mechanisms in search of treatments. Neuron 67:181–198. CrossRef Medline

Muñoz-Fontela C, Macip S, Martínez-Sobrido L, Brown L, Ashour J, García-Sastre A, Lee SW, Aaronson SA (2008) Transcriptional role of p53 in interferon-mediated antiviral immunity. J Exp Med 205:1929–1938. CrossRef Medline

Noriega LG, Feige JN, Canto C, Yamamoto H, Yu J, Herman MA, Mataki C, Kahn BB, Auwerx J (2011) CREB and ChREBP oppositely regulate SIRT1 expression in response to energy availability. EMBO Rep 12:1069–1076. CrossRef Medline

Ousman SS, Wang J, Campbell IL (2005) Differential regulation of interferon regulatory factor (IRF)-7 and IRF-9 gene expression in the central nervous system during viral infection. J Virol 79:7514–7527. CrossRef Medline

Outeiro TF, Kontopoulos E, Altmann SM, Kufareva I, Strathearn KE, Amore AM, Volk CB, Maxwell MM, Rochet JC, McLean PJ, Young AB, Abagyan R, Feany MB, Hyman BT, Kazantsev AG (2007) Sirtuin 2 inhibitors rescue alpha-synuclein-mediated toxicity in models of Parkinson's disease. Science 317:516–519. CrossRef Medline

Paraíso AF, Mendes KL, Santos SH (2013) Brain activation of SIRT1: role in neuropathology. Mol Neurobiol 48:681–689. CrossRef Medline

Paun A, Pitha PM (2007) The IRF family, revisited. Biochimie 89:744–753. CrossRef Medline

Raz L, Zhang QG, Han D, Dong Y, De Sevilla L, Brann DW (2011) Acetylation of the pro-apoptotic factor, p53 in the hippocampus following cerebral ischemia and modulation by estrogen. PLoS One 6:e27039. CrossRef Medline

Savitz SI, Schäbitz WR (2008) A critique of SAINT II: wishful thinking, dashed hopes, and the future of neuroprotection for acute stroke. Stroke 39:1389–1391. CrossRef Medline

Schmued LC, Hopkins KJ (2000) Fluoro-Jade B: a high affinity fluorescent marker for the localization of neuronal degeneration. Brain Res 874:123–130. CrossRef Medline

Takaoka A, Hayakawa S, Yanai H, Stoiber D, Negishi H, Kikuchi H, Sasaki S, Imai K, Shibue T, Honda K, Taniguchi T (2003) Integration of interferon-alpha/beta signalling to p53 responses in tumour suppression and antiviral defence. Nature 424:516–523. CrossRef Medline

Tamura T, Yanai H, Savitsky D, Taniguchi T (2008) The IRF family transcription factors in immunity and oncogenesis. Annu Rev Immunol 26:535–584. CrossRef Medline

Taniguchi T, Takaoka A (2002) The interferon-alpha/beta system in antiviral responses: a multimodal machinery of gene regulation by the IRF family of transcription factors. Curr Opin Immunol 14:111–116. CrossRef Medline

Tsuno T, Mejido J, Zhao T, Schmeisser H, Morrow A, Zoon KC (2009) IRF9 is a key factor for eliciting the antiproliferative activity of IFN-alpha. J Immunother 32:803–816. CrossRef Medline

Tymianski M (2011) Emerging mechanisms of disrupted cellular signaling in brain ischemia. Nat Neurosci 14:1369–1373. CrossRef Medline

Vaseva AV, Marchenko ND, Ji K, Tsirka SE, Holzmann S, Moll UM (2012) p53 opens the mitochondrial permeability transition pore to trigger necrosis. Cell 149:1536–1548. CrossRef Medline

Vaziri H, Dessain SK, Ng Eaton E, Imai SI, Frye RA, Pandita TK, Guarente L, Weinberg RA (2001) hSIR2(SIRT1) functions as an NAD-dependent p53 deacetylase. Cell 107:149–159. CrossRef Medline

Vosler PS, Chen J (2009) Potential molecular targets for translational stroke research. Stroke 40:S119–S120. CrossRef Medline

Wang L, Deng S, Lu Y, Zhang Y, Yang L, Guan Y, Jiang H, Li H (2012a) Increased inflammation and brain injury after transient focal cerebral ischemia in activating transcription factor 3 knockout mice. Neuroscience 220:100–108. CrossRef Medline

Wang L, Lu Y, Deng S, Zhang Y, Yang L, Guan Y, Matozaki T, Ohnishi H, Jiang H, Li H (2012b) SHPS-1 deficiency induces robust neuroprotection against experimental stroke by attenuating oxidative stress. J Neurochem 122:834–843. CrossRef Medline

Wang L, Lu Y, Guan H, Jiang D, Guan Y, Zhang X, Nakano H, Zhou Y, Zhang Y, Yang L, Li H (2013a) Tumor necrosis factor receptor-associated factor 5 is an essential mediator of ischemic brain infarction. J Neurochem 126:400–414. CrossRef Medline

Wang L, Lu Y, Zhang X, Zhang Y, Jiang D, Dong X, Deng S, Yang L, Guan Y, Zhu L, Zhou Y, Zhang X, Li H (2013b) Mindin is a critical mediator of ischemic brain injury in an experimental stroke model. Exp Neurol 247:506–516. CrossRef Medline

Wang P, Xu TY, Guan YF, Tian WW, Viollet B, Rui YC, Zhai QW, Su DF, Miao CY (2011) Nicotinamide phosphoribosyltransferase protects against ischemic stroke through SIRT1-dependent adenosine monophosphate-activated kinase pathway. Ann Neurol 69:360–374. CrossRef Medline

Wang XA, Zhang R, Jiang D, Deng W, Zhang S, Deng S, Zhong J, Wang T, Zhu LH, Yang L, Hong S, Guo S, Chen K, Zhang XF, She Z, Chen Y, Yang Q, Zhang XD, Li H (2013) Interferon regulatory factor 9 protects against hepatic insulin resistance and steatosis in male mice. Hepatology 58:603–616. CrossRef Medline

Xia CF, Smith RS Jr, Shen B, Yang ZR, Borlongan CV, Chao L, Chao J (2006) Postischemic brain injury is exacerbated in mice lacking the kinin B2 receptor. Hypertension 47:752–761. CrossRef Medline

Yanai H, Negishi H, Taniguchi T (2012) The IRF family of transcription factors: inception, impact and implications in oncogenesis. Oncoimmunology 1:1376–1386. CrossRef Medline

Yenari MA, Han HS (2012) Neuroprotective mechanisms of hypothermia in brain ischaemia. Nat Rev Neurosci 13:267–278. CrossRef Medline

Zhou S, Chen HZ, Wan YZ, Zhang QJ, Wei YS, Huang S, Liu JJ, Lu YB, Zhang ZQ, Yang RF, Zhang R, Cai H, Liu DP, Liang CC (2011) Repression of P66Shc expression by SIRT1 contributes to the prevention of hyperglycemia-induced endothelial dysfunction. Circ Res 109:639–648. CrossRef Medline

Zhu HR, Wang ZY, Zhu XL, Wu XX, Li EG, Xu Y (2010) Icariin protects against brain injury by enhancing SIRT1-dependent PGC-1alpha expression in experimental stroke. Neuropharmacology 59:70–76. CrossRef Medline